PERFORMANCE OF SHALLOW ANCHOR IN ICE-RICH SILT

By

Chuang Lin

RECOMMENDED:

Mr. Billy Connor

Dr. Jenny Liu

Dr. Yuri Shur

Dr. Xiong Zhang
Advisory Committee Chair

Dr. Robert Perkins
Chair, Department of Civil and Environmental Engineering

APPROVED:

Dr. Douglas J. Goering
Dean, College of Engineering and Mines

Dr. John Eichelberger
Dean of the Graduate School

12/15/14
Date

PERFORMANCE OF SHALLOW ANCHOR IN ICE-RICH SILT

A

THESIS

Presented to the Faculty

of the University of Alaska Fairbanks

in Partial Fulfillment of the Requirements

for the Degree of

MASTER OF SCIENCE

By

Chuang Lin, B.E.

Fairbanks, AK

December 2014

ABSTRACT

Shallow anchor systems have been widely used for decades due to their time and cost efficiency. Yet when it comes to cold regions like Alaska, new challenges caused by the harsh environment need to be resolved before they are used extensively in cold regions. One challenge associated with anchor installation could be the potential thawing of warm permafrost due to the grout mortar hydration, which might undermine the capacity of the anchor. Another challenge is that due to low temperature the grout may cure slower or not cure at all, which will also result in a significant decrease in the ultimate strength of the anchor.

Field tests were conducted to evaluate the performance of shallow anchors including duckbill anchors and grouted anchors with three types of different grouting materials, including Microsil Anchor Grout, Bentonite Clay and a newly-developed Antifreeze Grout Mortar. Constant-load creep test and pullout test were conducted to evaluate the performance of the anchors.

Test results indicated that the anchors grouted with Antifreeze Grout Mortar caused the least permafrost disturbance and degradation, gained the largest tensile strength, exhibited the least creep displacement, and showed relatively large pullout capacity, and thus achieved the best performance among all types of shallow anchors.

TABLE OF CONTENTS

Page

Page

LIST OF FIGURES

Page

Page

LIST OF TABLES

Page

ACKNOWLEDGEMENTS

I would like to express my sincere gratitude to my advisor, Dr. Xiong Zhang, Associate Professor of Civil Engineering, University of Alaska Fairbanks, for serving as my committee chair. I am very grateful for his indispensable guidance and continuous support.

I want to extend special thanks to Dr. Jenny Liu, Associate Professor of Civil Engineering, University of Alaska Fairbanks, Dr. Yuri Shur, Professor of Civil Engineering, University of Alaska Fairbanks, and Mr. Billy Connor, Director of Alaska University Transportation Center, for being committee members. They took enormous time for discussions on the project and spent considerable time reviewing the thesis. Their precious suggestions and comments are highly appreciated. I would also like to thank Mr. Robert Mchattie, Consultant of GZR Engineering, for reviewing the project report and providing valuable suggestions.

I am grateful to Gary Tyndall, Lab Manager of Department of Civil Enginering, University of Alaska Fairbanks, Joel Bailey, Research Professional, Institute of Northern Engineering, and Kelvin Bjella, Director of Cold Regions Research and Engineering Laboratory. Their supports on the experimental research of anchors are highly appreciated.

Special thanks are extended to Alaska University Transportation Center, Alaska Department of Transportation & Public Facilities, Institute of Northern Engineering, and Department of Civil and Environment Engineering for the funding of the project and financial support during my studies.

And finally, I would like to thank my family for their encouragement and support. And also thanks are expressed to those friends, Lin Li and Kai Wang for their help in the permafrost tunnel.

CHAPTER 1 INTRODUCTION

1.1 PROBLEM STATEMENT

Grouted anchors and anchored systems have been successfully for over 50 years as time and cost effective soil supporting systems for earth retention, slope stability and tie-down structure projects. Compared with conventional earth retention systems, grouted anchor systems have several benefits. The construction workspace is small and the time consumed for installing a grouted anchor is relatively less. A grouted anchor also provides a comparatively large amount of resistant strength considering the amount of material used. Moreover, temporary supports are not required in many anchor-type systems, thus providing cost savings over most other systems. The theory for the application of grouted anchors in unfrozen soil has been explored for several decades, and discussions regarding the load transfer mechanism, group effect and its application to different types of soils can be found in a series of published papers (Adams and Hayes, 1967; Bhatnagar, 1969; Adams and Klym, 1972; Das, 1975; Casanovas, 1989; Barley, 1997; Adams and Littlejohn, 1997; Briaud et al., 1998; Rollins et al., 2005; Hanna et al., 2007; Hsu, 2012).

Permafrost exists extensively in cold regions. Figure 1.1 shows the permafrost distribution in Alaska. Nearly 80% of the Alaska region covers with either continuous or discontinuous permafrost. The application of grouted anchors in permafrost areas inevitably encounters many new issues and challenges. One challenge is that the grout may cure slower or cannot cure at all due to the low temperature, which will result in a significant decrease in the ultimate strength of the grout. Limited references can be found regarding the development of innovative grout mortar suitable for cold regions (Biggar and Sego, 1990; Biggar et al., 1991 and Johnston and Ladanyi, 1972). In general, high alumina cements (such as Ciment Fondu) were the most commonly used grouts in cold regions. Yet, the degradation of the frozen soil was not evaluated in the previous research. Whether this type of cement is applicable to lower temperatures and whether there is a better solution still need to be explored.

Another challenge associated with anchor installation could be the potential thawing of the warm permafrost due to grout mortar hydration, which might elongate the construction period and undermine the capacity of the anchor. It is of large significance to come up with a special type of

grout mortar with excellent flowability for grouting, depressed freezing point of mix water, and accelerated early-age strength at low temperature.

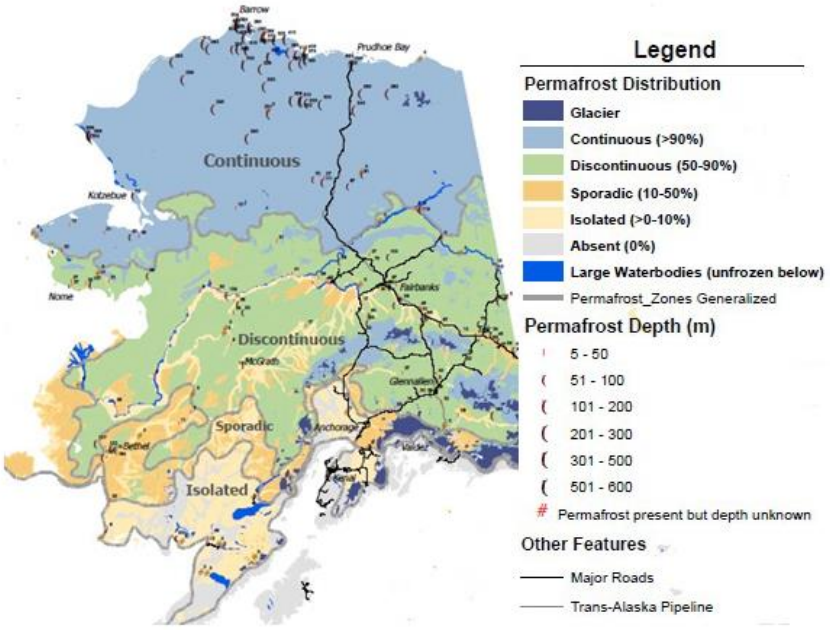

Figure 1.1 Permafrost Distribution Map of Alaska (Jorgenson et al., 2008)

Furthermore, the creep behavior of anchor is one of the major concerns for anchor design in cold regions. Compared with unfrozen soils, the existence of ice in frozen soil makes it even more difficult to evaluate the creep behavior and to analyze the load transferring mechanism along the anchor shaft. Published papers describing the strength and creep behavior for frozen soils are relatively limited (Glen, 1955; Ladanyi and Johnston, 1974; Nixon and McRoberts, 1976; Nixon, 1988; Biggar and Sego, 1993a, b; Biggar and Kong, 2001; Andersland and Ladanyi, 2004; Arenson and Springman, 2005). The creep behavior of ice-rich frozen soils varies with different temperatures and ice contents. Bray (2008) observed different creep behaviors of undisturbed and remolded Fairbanks silt, and limited field test data could be found to further explain this variation. Moreover, the existing studies of anchors in cold regions consider the anchor as a whole to analyze the load transferring mechanism, rather than to separate the anchor tendon and grout independently. Therefore, it is also important to collect the field creep data for undisturbed Fairbanks silt for further research and explore the load transferring mechanism within both anchor tendon and grout.

1.2 RESEARCH OBJECTIVES

Based on the problems stated in Section 1.1, the major objective of this study is to evaluate the performance of different types of anchors in cold regions. And the following aspects are critical for the performance of grouted anchors and become the primary considerations for the evaluation:

1. Exploring the creep behavior of different types of anchors in ice-rich silt;
2. Analyzing the load distributions along the anchor shaft;
3. Evaluating the permafrost degradation induced by hydration heat;
4. Comparing the pullout capacity for different types of anchors.

1.3 RESEARCH METHODOLOGY

In order to achieve the research objectives, the following tasks are conducted:

1. Literature review

Chapter 2 provides a comprehensive literature review of previous research on grouted anchors and creep behavior, with focus on those performed in permafrost areas. The review provides essential background information on creep theory of ice and ice-rich soils, factors that influence the creep behavior of grouted anchors and previous studies on load transferring mechanism.

2. Field Test

Chapter 3 discusses field testing of 13 grouted anchors and 4 duckbill anchors. These anchors were installed into ice-rich permafrost soils at a site near Fox, Alaska. Details of the field site are introduced in this chapter. Then the testing equipment is discussed including sensor, loading system and data acquisition system. After that, test preparations such as borehole drilling processes, sensor installation procedures, and grouting material preparation are presented. Finally, both the testing procedures of duckbill and grouted anchors are provided in this section.

3. Test Results and Data Analyses

Chapter 4 presents test results and data analyses. The performance of duckbill anchors is discussed first. Then the effect of hydration heat on permafrost degradation is evaluated. Finally, the creep and pullout test results are presented and analyzed.

4. Summary and Recommendation

Chapter 5 gives a summary of the test results and conclusions based on Tasks 1 through 3. Recommendations are offered regarding the use of shallow anchors in ice-rich permafrost.

CHAPTER 2 LITERATURE REVIEW

In this chapter, background information about creep behavior of ice and frozen soils are first presented. Then, grouted anchor design considerations in permafrost area are reviewed. Finally, a review of the development of load distribution analysis is discussed.

2.1 CREEP THEORIES FOR ICE AND FROZEN SOILS

Creep is the tendency of a solid material to deform slowly under the influence of mechanical stresses. It can occur as a result of long-term exposure to high levels of stress that are still below the yield strength of the material. Creep is more severe in materials that are subjected to heat for long periods, and generally increases as they near their melting point (wikipedia.org). It is well-established ice and frozen soils creep under warm temperatures. The overall creep behavior of grouted anchors under constant load at constant temperature is shown in Figure 2.1.

In general, three distinguishing stages can are identified from the figure:

1. Primary creep: displacement increases with time while the displacement rate decreases gradually with time.
2. Secondary creep: this stage is also called steady-state creep, and the displacement rate remains constant.
3. Tertiary creep: displacement rate increases rapidly with time. The onset of the tertiary stage is always considered the beginning of failure.

Creep curves plotted for each anchor or pile show distinct primary, secondary and tertiary stages under different load levels, loading rates, soil types and temperatures. At higher loads anchors exhibit a short secondary stage, and the tertiary stage will not appear at very low load levels (Johnston and Ladanyi, 1972).

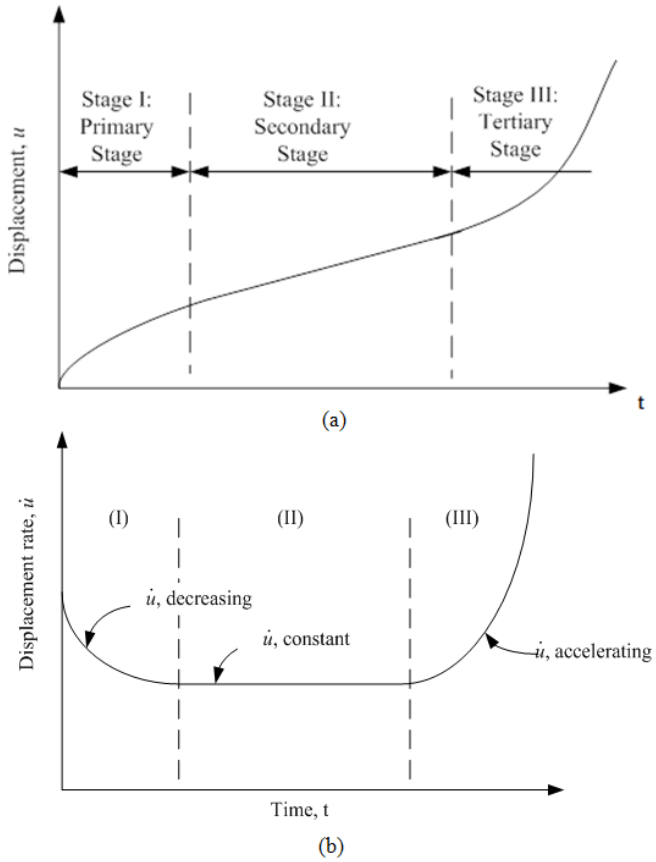

Figure 2.1 Creep Behavior of Grouted Anchors
(After Vialov et al., 1962; Biggar and Kong, 2001)

2.1.1 Creep Behavior of Ice

For ice-rich permafrost, the frozen soil contains large portion of ice. So the study of the creep behavior of ice-rich permafrost was actually originated from the study of the creep behavior of pure ice. Glen (1952, 1955) was one of the first researchers to conduct comprehensive creep tests on polycrystalline ice. The test results indicated that ice behaved similar to metals, which are also crystalline materials. Thus a simple power law was proposed to describe such creep behavior, as shown in Equation (2.1):

$$\dot{\varepsilon} = A\sigma^{n} \tag{2.1}$$

where $\dot{\varepsilon}$ is axial strain rate; σ is axial stress; A is the parameter dependent on temperature and ice type; and *n* is the experimentally derived exponent.

Shreve and Sharp (1970) reported results which indicated a good match with Glen's simple flow law. Moreover, Raymond (1971) used three-dimensional velocity distribution to interpret the field data of glacier ice and validated the method of using a simple power law under low stress conditions. Yet, the tests performed by Glen were under relatively high stress levels, which did not fit the actual geotechnical engineering problems. For tests using lower stress states at temperatures near the melting point, the exponent *n* was much higher. Butkovich and Landauer (1959, 1960) observed the viscous behavior of ice near melting point (32°F or 0°C) at low stress levels. The test results indicated that some variations occurred in the flow law parameters for the various ice types. However, the general format of the flow law under different stress states was similar. Mellor and Testa (1969) developed a constitutive relationship, which extended predictions of secondary creep through a broader range of stress.

Barnes et al. (1971) assumed that the creep behavior of polycrystalline ice consisted of three components: elastic strain, transient strain and steady-state strain. Based on the assumption, another constitutive equation was introduced, as shown in Equation (2.2) as follows:

$$\varepsilon = \varepsilon_0 + \beta t^{\frac{1}{3}} + \dot{\varepsilon} t \tag{2.2}$$

where ε is total strain; ε_0 is instantaneous elastic strain; β is the constant for transient creep; $\dot{\varepsilon}$ is the steady-state creep rate; and t is time.

This equation enabled the secondary creep rate to be defined for a wide range of temperatures and stresses by extracting the steady-state strain rate from the short-term, low stress tests. Several researchers (Budd, 1969; Paterson and Savage, 1963) also performed tests with the temperature near melting point and under low stress. But their test results were difficult to interpret. The equation proposed by Thomas (1973) for describing the creep behavior of floating ice shelves was in good agreement with the Barnes et al.'s (1971) laboratory test results under a higher stress state. He reduced some of the difficulties in interpreting the deformation of glacier ice, by assuming well-defined upper and lower surfaces that remained uniform over a relatively long distance. The good agreement of results from field and laboratory tests enabled a better understanding of the flow law of ice under low stresses.

2.1.2 Creep Behavior of Frozen Soil

Vialov (1959) was one of the first researchers who systematically studied the strength and stability of frozen soils. He pointed out that one of the most important characteristics of frozen soil was the time- and temperature-dependent constitutive relationship. Frozen soil contained both the solid and liquid phase of water. Vialov noticed that the behavior of frozen soil was significantly affected by rheological deformation when the temperature was close to the melting point. The soil exhibited a highly plastic-viscous property, which meant that the strength of the frozen soil would decrease rapidly under the influence of load. Furthermore, Vialov et al. (1962) presented the stress-strain relationship based on the test results from undisturbed sandy silts and clays. The formula is as follows:

$$\varepsilon = \left[\frac{\sigma \cdot t^{\lambda}}{\omega(\theta+1)^{k}}\right]^{\frac{1}{m}} + \varepsilon_0 \tag{2.3}$$

where σ is applied stress; t is time; θ is temperature (°C) below the freezing point; ε_0 is instantaneous strain; and λ, m, ω, and k are constant parameters that represent the property of materials.

Sayles (1968) proved the Vialov's strength formula by studying the creep stress-strain relationship of frozen Ottawa sand and Manchester fine sand at various temperatures. The content of unfrozen water in frozen sand was very small so that the effect of unfrozen water on the strength of frozen sand could be neglected. Similar assumption was adopted by Butkovich (1954).

Johnston and Ladanyi (1972) conducted both constant and step load tests of grouted piles in two permafrost field sites near Manitoba, Canada. Johnston and Ladanyi also provided a method for predicting the long-term adfreeze strength of frozen soil based on the engineering creep theory. The estimated value of long-term adfreeze strength fitted well with the field test results. The normalized creep rate is as follows:

$$\frac{\dot{U}_a}{a} = \frac{3^{(n_1+1)/2} B_1 {\tau_a}^{n_1}}{n_1 - 1} \tag{2.4}$$

where $\dot{U}_a$ is the steady-state creep rate at radius of a; a is the distance from the axis of the anchor; n_1 and B_1 are creep parameters related to the property of pile and temperature; and τ_a is shear stress at a distance of a.

A number of researchers, such as Nixon and McRoberts (1976), Weaver (1979) and Morgenstern et al. (1980), conducted both laboratory and field tests to predict the creep behavior of piles in different frozen soils. The redistribution of stress along the pile was found to occur prior to the onset of the secondary creep state. Plus, the time for reaching a uniformly distribution of stress was significantly affected by ground temperature and varied from 1 day to 1 year. Moreover, it was assumed by all the researchers that the soil deformation was continuous, which indicated a homogeneous soil, and that the shear strain rate remained constant as long as the applied stress did not surpass the pile's adfreeze strength.

Parameswaran (1986) performed a series of tests on small-scale model piles in different frozen soils by using Constant Rate Test (CRT) and Constant Load Test (CLT). The test results indicated that Vialov's method of predicting the bearing capacity could result in a much higher allowable strength value compared with the results obtained by Parameswaran from constant load tests. However, he also admitted that Vialov's method gave a convenient way of estimating the long-term pile bearing capacity in permafrost.

Nixon and Neukirchner (1984) reported significantly reduced pile capacity due to the increase of salinity in frozen ice-rich soil. Their study indicated that the temperature dependent exponent *n* would decrease with increasing salinity. Biggar (1991) pointed out that saline fluid in contact with the surface of pile would result in the reduction of the adfreeze bond strength during the freezing process. Biggar and Sego (1993a) performed studies on creep models for piles in frozen saline soil and concluded that a the creep law for piles in ice-poor frozen saline silt sand could be described adequately by a simple power law to predict short-term pile displacement. For the long-term displacement of piles, a flow law would be a better way of predicting the displacement.

2.2 GROUTED ANCHOR DESIGN CONSIDEARTIONS

2.2.1 Temperature

The creep behavior of frozen soil is significantly dependent on temperature. In general, the creep displacement rate decreases dramatically with the decrease in temperature. Morgenstern et al. (1980) reported that the displacement rate at 14°F (-10°C) was 10-100 times smaller than that at 30.2°F (-1°C), given the same shear stress and pile dimensions. When the temperature was near the freezing point (32°F or 0°C), the displacement rate increased significantly. Biggar and Sego (1993a) also reported significant displacement rate increase with an increase of of only 1.8°F (1°C) in temperature.

In general, it is thought that the existence of soil particles will impede the dislocation of ice crystals and thereby minimize the creep rate. A contrasting general assumption held by some researchers is that the presence of soil particles, at low concentration, will reduce friction between ice crystals and therefore accelerate the creep rate. However, results of long-term creep tests, conducted at temperatures near the freezing point by Thompson and Sayles (1972), Roggensack (1977), and McRoberts et al. (1978), suggested that the creep behavior of frozen soil (especially near the freezing point) is a more complicated process. Thompson and Sayles's results with Fairbanks silt indicated that the creep rate of silt is comparable to that of polycrystalline ice. Yet, McRoberts et al. (1978) reported that the Norman Wells Silt exhibited a lower creep rate than polycrystalline ice, while Roggensack (1977) observed a lower creep rate than polycrystalline ice. In a summary, the creep behavior of frozen soils near melting point may vary from one type to another.

The thermal gradient is another consideration in permafrost areas. In general, the thermal gradient of greater than 30 m/°C can be expected in many permafrost areas. Thus, it is reasonable to assume that the temperature along the anchor shaft is uniformly distributed.

2.2.2 Soil Type

It is recognized that fine-grained frozen soils often exhibit a rheological and viscous character. Such material can be categorized into two types: ice-poor and ice-rich frozen soil. The long-term deformation of fine-grained ice-rich soil is dominated by secondary creep, while the deformation of ice-poor fine-grained soil is controlled by primary creep. In previous designs of anchors or

piles in such soils, adfreeze bond strength has been the major concern. Yet, it is prudent that the creep behavior of ice-rich fine-grained soils be accounted for by a design approach such as that based on limiting deformation. Nixon and McRoberts (1976) and Morgenstern et al. (1980) did such design-related predictions based on the flow law of ice.

2.2.3 Cement

Cement used for applications where it is in contact with permafrost soils is quite different from that used for unfrozen soil applications. Installation of anchors in frozen soil also poses new challenges for grouting material. Cement is usually used as grout material for anchor applications. Cement used in frozen soil applications should be kept from freezing until the hydration process is complete. Mixtures of cement-based materials used in a permafrost soil environment must have sufficient bond strength for the intended application. The material must possess handling properties that allow for simple and easy placement, assuming adverse environmental conditions at the time of construction. Additionally, it is necessary that the cement-based material generate minimal heat during the hydration process, as such heat will degrade the permafrost.

Five types of cement systems were tested by Biggar and Sego (1993a). The first one was neat Ciment Fondu. Test results indicated that temperatures remained above the freezing point until the hydration reaction subsided. The ice-cement interface experienced a temperature increase of only 3.6°F (2°C). The final compression strength was 3160 psi (21787 KPa). The second type was Fondu: Fly Ash (50:50). Test results showed a curing temperature lower than the first type, but high enough for the system to set and achieve the final compression strength of 1796 psi (12383 KPa). The third cement type was Gypsum: Portland Cement (50:50) with 20% of the mixing water replaced by alcohol to lower the freezing point during hydration. Test results indicated that no bond developed between ice and pile even though the cement mixture cured. The fourth type was Gypsum: Portland Cement (50:50) with 18% sodium chloride by weight of mix water to depress the freezing point. This type of cement system exhibited a higher increment in temperature during hydration that lasted for only a short time, but the final bond was not strong. The fifth and last type was API Class C Cement with 2% calcium chloride. This cement performed worst with 50% of cement frozen, but with no temperature increase.

Yet, no detailed field test data was available to evaluate the potential thawing of the surrounding permafrost due to grout mortar hydration. It is of great importance to develop an effective Antifreeze Grout Mortar for the successful application of anchors in cold regions.

2.2.4 Properties of Backfill Materials

Properties of backfill materials affect the load capacity of anchors and piles greatly. The adfreeze bond strength governs the load capacity of anchors and piles by controlling the level of shear strength that can develop between these structures and the frozen backfill material. Also, piles and anchors with rough surfaces provide the additional contact area that of course increases total area of the adfreeze bond. The additional adfreeze bond developed over the additional (rough) area means that total shear strength and therefore total load capacity increase.

Sego and Smith (1989) performed laboratory tests at 23°F (-5°C) with various backfill materials. The backfill materials used in the research were clean sand slurry, silty sand slurry, silty saline sand slurry, and ice. Comparison with the test results for nonsaline backfill materials found that similar short-term pile adfreeze strengths were achieved regardless of the silt content. Comparisons between ice and nonsaline sand backfill found that the ice generated 40% less adfreeze strength. Another test, which looked at pile surface treatment, showed that it also played an important role in the short-term capacity of piles. Three types of pile surface were used in the test: an uncoated pile, a pile coated with black lacquer, and a pile with a sandblasted surface. The maximum short-term strength was achieved by the pile with a sandblasted surface due to the increased roughness of the pile surface.

2.2.5 Salinity

Anchor or pile capacity will dramatically decrease with the increase of salinity in frozen soil. Nixon and Neukirchner (1984) reported this phenomenon in their study of ice-rich frozen soil. The same test result was shown in the test of ice-poor frozen soil conducted by Biggar and Sego (1993a). The reason for this significant decrease in anchor or pile capacity is that unfrozen saline pore fluid is in direct contact with the pile surface, thereby diminishing the quality of the adfreeze bond (Nixon 1988; Hutchinson 1989). This indicates that the solute diffused from the native soil (or contained in the grouting material) and redistributed along the pile or anchor surface would limit adfreeze bond strength. Sego and Smith (1989) also compared test results for

nonsaline and saline backfill materials, and reported a 47% decrease in pile capacity due to salinity. Their research tends to confirm that salinity would be one of the major factors controlling the pile bearing capacity.

2.3 LOAD DISTRIBUTION OF GROUTED ANCHOR

Vesic (1969) proposed that the failure mode also played an important role in analyzing the load distribution process along the anchor shaft. Three cases were demonstrated in his research, including general shear failure with fully developed sliding surface and failure load, local shear failure where the lateral compression occurs with mobilized shear strength of the soil, and punching failure where only a lateral compression occurs.

In general, there are two major methods to analyze the load distribution along the anchor shaft: elastic solutions and numerical solutions. The elastic solutions were the earliest and most simplified methods. Mindlin (1936) derived the stress-strain relationship for anchor embedded in semi-infinite elastic medium. D'Appolonia and Romualdi (1963) performed tests on end-bearing H-piles that were driven to weathered shale based on this method. Yet, those test results were greatly affected by three factors: lateral earth pressure coefficient, Young's modulus of soil and elastic-plastic tip movement. Poulos and Davis (1968), Mattes (1969), and O'neil and Reese (1970) summarized and presented the elastic solution to determine load transfer mechanism based on Mindlin's method. Yet, all of the elastic solutions could not solve nonlinearity, nonhomogeneity, and time-dependent stress-strain problems, which are important characteristics of frozen soils.

Thanks to the significant improvement in computer technology, nowadays it is possible to solve those complicated problems that discussed above by mathematical simulation. Ellison et al. (1971), Desai (1974) compared the measured and predicted test results of various pipe piles with lengths ranging from 30 to 50 ft (9.1 to 15.2 m). Accurate results could be obtained with proper simulation of the soil properties. After that, more and more researchers started to use finite element method to predict the load distribution along anchors and piles. Cook et al. (1998), Subramanian and Cook (2002, 2004) also analyzed the failure modes of single adhesive anchors under tensile load.

The group effect on the load distribution of piles can be seen in numbers of papers (Butterfield and Banerjee, 1971; Randolph and Wroth 1979; Mylonakis and Gazetas, 1998; Leung et al., 2010). A variety of approaches were adopted, such as boundary element methods, hybrid load transfer approach and finite element method.

CHAPTER 3 FIELD TESTS

3.1 TEST SITE DESCRIPTION AND ANCHOR CONFIGURATION

Field testing was conducted in the US Army Cold Region Research and Engineering Laboratory (CRREL) permafrost tunnel located at Fox, Alaska, which is located 16 miles north of Fairbanks. Previous study indicates that this area belongs to a discontinuous permafrost region, which is sensitive to thermal disturbance. The tunnel is composed of two parts, as shown in Figure 3.1. One is the nearly horizontal main adit from the entrance to the hill side and the other is the inclined adit which is denoted as "winze". According to the guidebook of the CRREL permafrost tunnel, the main adit of the tunnel is approximately 360 ft (110 m) long, 6.6 to 8.2 ft (2.0 to 2.5 m) high, and 13.1 to 16.4 ft (4.0 to 5.0 m) wide. The winze is about 147.6 ft (45.0 m) in length, beginning about 65.6 ft (20.0 m) from the tunnel entrance, and drops at an incline of 14° passing through the gravel unit and finally reaching the weathered bedrock.

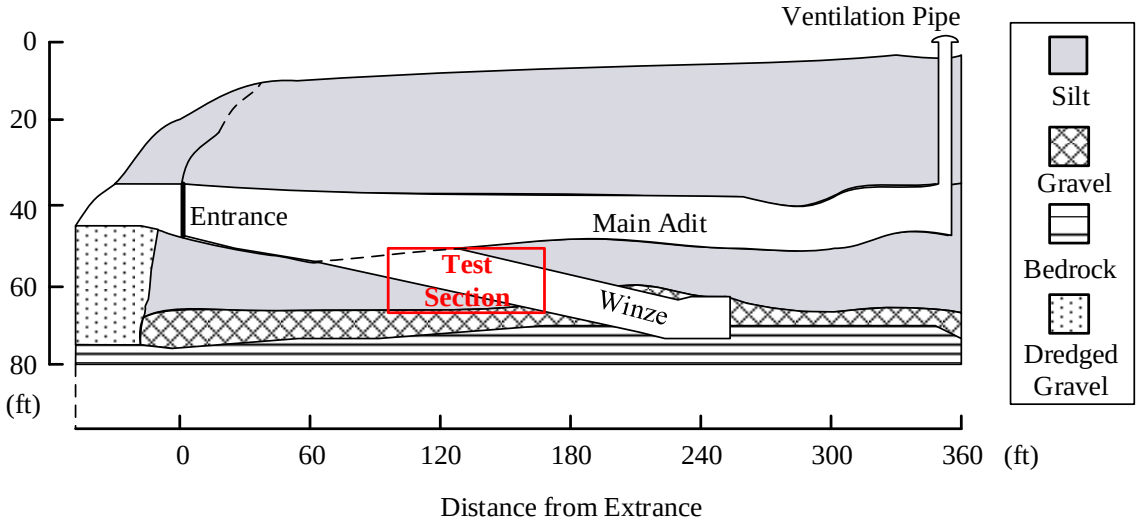

Figure 3.1 Schematic Plot of CRREL Permafrost Tunnel

The field test zone is at the right-hand side of the tunnel, beginning at 108 ft (33 m) from the entrance side and ending at 177 ft (54 m), as shown in Figure 3.2. In total, 17 boreholes were drilled within the test section, including 13 grouted anchor boreholes and 4 duckbill anchor boreholes. The test section is divided into 5 zones to test different types of anchors, including duckbill anchors (13, 14, 16 and 17), hollow anchor tendon grouted with Antifreeze Grout

Mortar (11, 12 and 15), with Bentonite Clay (8, 9 and 10), with Microsil Anchor Grout (5, 6 and 7), and also solid anchor tendon grouted with Microsil Anchor Grout (1, 2, 3 and 4).

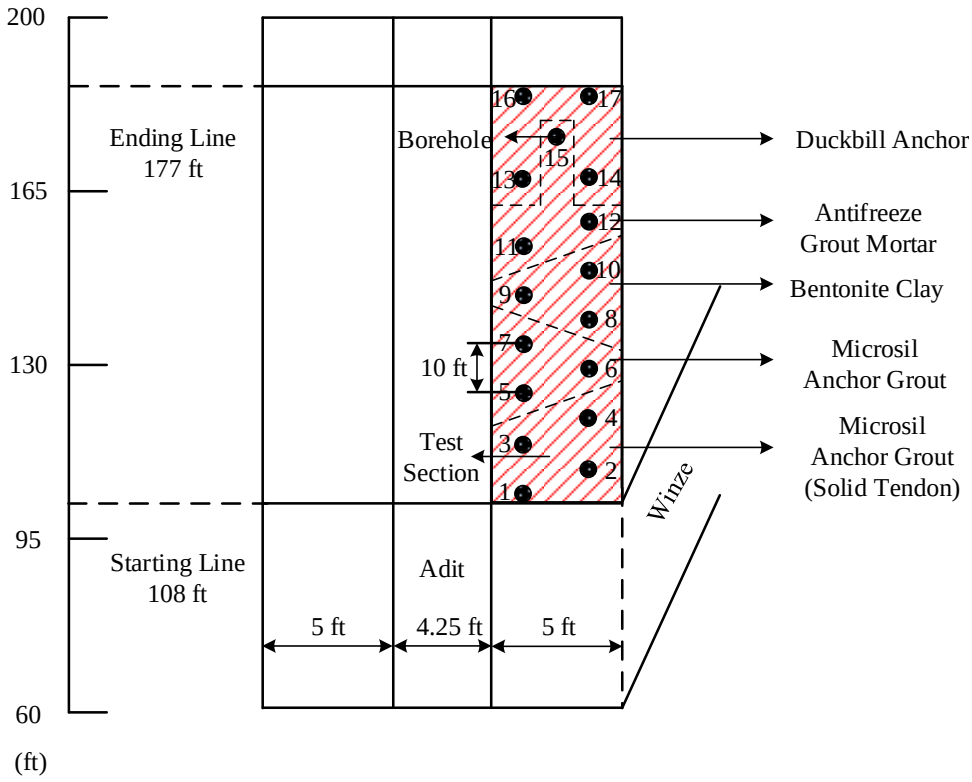

Figure 3.2 Test Section and Anchor Layout

Also, the layout of each anchor, and the soil profile beneath the test section, are shown in Figure 3.3. Two types of sensors are used including: Geokon vibrating wire strain gages to measure the strain in grout, and HPI weldable strain gages to measure the strain in anchor tendon. The sensors are located at depths of 1.50 ft (0.46 m), 3.83 ft (1.17 m), 6.16 ft (1.88 m) and 8.50 ft (2.60 m), respectively. Detailed information about the boreholes and dimensions of anchors can be found in Section 3.3.1 and 3.3.2. Table 3.1 shows detailed information about the types of anchor tendon and grout, and sensors for each anchor.

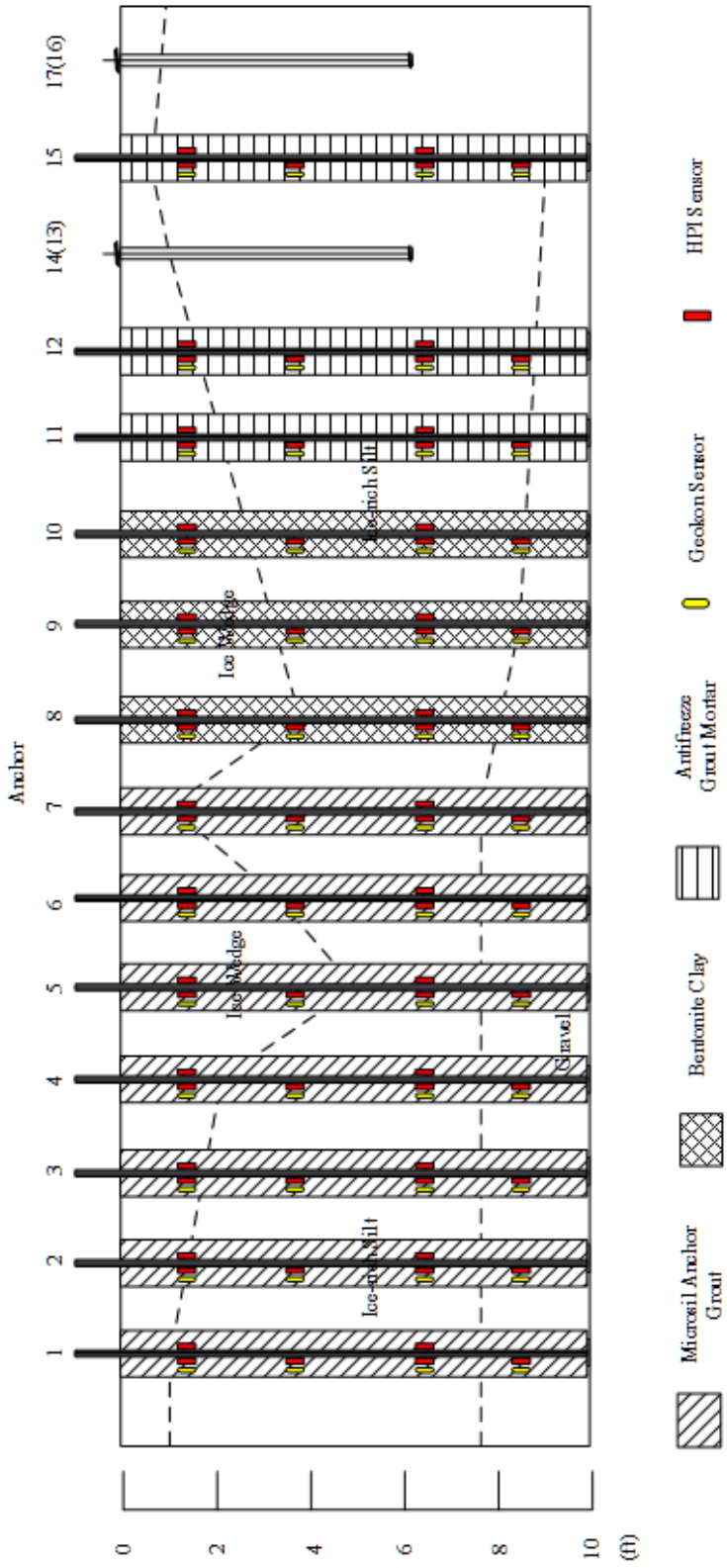

Figure 3.3 Schematic Plot of Soil Profile

Table 3.1 Detailed Anchor Information

		Anchor No.												
		1	**2**	**3**	**4**	**5**	**6**	**7**	**8**	**9**	**10**	**11**	**12**	**15**
Sensor	**HPI**	6	6	6	6	6	6	0	6	6	0	6	4	0
	Geokon	4	4	4	0	4	4	0	4	4	0	4	4	0
Rebar	**Solid**	X	X	X	X									
	Hollow					X	X	X	X	X	X	X	X	X
Grout	**MAG***	X	X	X	X	X	X	X						
	BC*								X	X	X			
	AGM*											X	X	X

*MAG: Microsil Anchor Grout; BC: Bentonite Clay; AGM: Antifreeze Grout Mortar

Based on the drilling log and previous studies (Kanevskiy et al., 2008), the ice content of sediments in the tunnel varies widely. The gravimetric moisture content of weathered schist (found in a portion of the winze called Gravel Room) ranges from 6.5% to 19.9%, averaging 11.7%. Sediments with an organic content of 9% to 12% may have gravimetric moisture content in the range of 70% to 80%. For modified sediments with structureless cryostructure, the gravimetric moisture content varies from 50% to 95% (Bray, 2008). In general, the Fairbanks silt in the test zone contains about 5%-10 % organic materials and less than 5% sand. The PL (Plastic Limit) and LL (Liquid Limit) for Fairbanks silt is 34% and 38%, respectively (Zhu and Carbee, 1987). According to Unified Soil Classification System (USCS), the soil beneath the test section shall be defined as low plasticity silt (ML).

3.2 TEST EQUIPMENT

3.2.1 Loading System

Figure 3.4 shows the testing system for the duckbill anchors. The major components include: weights, lever arm, steel chain, main beam, LVDT stand and flat steel bar. The main beam of the frame is supported by four columns and the lever consists of two channel beams. The lever arm ratio is 10:1 and bolted to the main beam by a flat plate. The steel chain connects the end of the lever arm with a hex nut on top of the anchor. The designed pullout capacity of the test frame is 3.5 tons (35.0 KN).

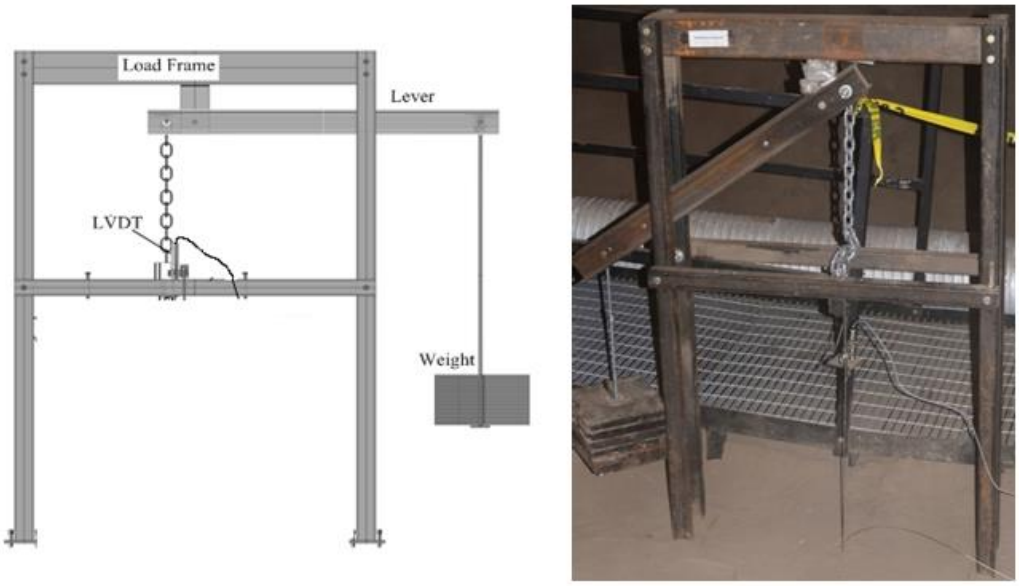

Figure 3.4 Loading System for Duckbill Anchors

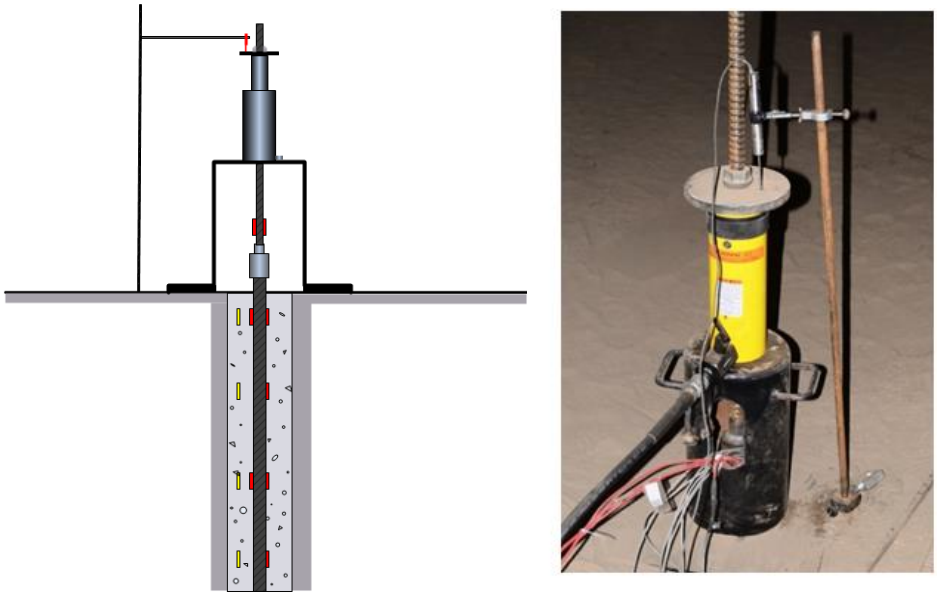

Figure 3.5 Loading System for Grouted Anchors

The loading system for grouted anchors, as shown in Figure 3.5, consists of an Enerpack hydraulic jack, hydraulic pump, base, iron plate, and nut. The hydraulic jack is 6.13 in (155 mm) in height, and the outer and inner diameters are 4.50 in (114 mm) and 1.31 in (33 mm), respectively. The hydraulic jack sits on the base and is fastened by an iron plate with a nut on the top. The applied load is transferred to the anchor through the couple. An LVDT is placed on top of the iron plate to monitor the displacement of the anchor, and the LVDT holder is hammered to

the frozen ground. Two hydraulic jacks are connected to the pump through hydraulic tubes (two anchors can be tested simultaneously), as shown in Figure 3.6. The maximum pressure provided by the hydraulic jack is 10000 psi (68947 KPa) with an accuracy of 200 psi (1379 KPa). The hydraulic jack has a capacity of 30 tons (300 KN) and effective area is 7.22 in^2 (4658.06 mm^2). The hydraulic pump provides hydraulic pressure through a main pressure control switch (gauge 1) to a manifold that offers two hydraulic line attachment points (gauge 2 and 3), each with the capability of independent pressure control. Therefore, it is possible for the single pump to simultaneously supply two jacks with the correct hydraulic pressures needed for maintaining two different loads.

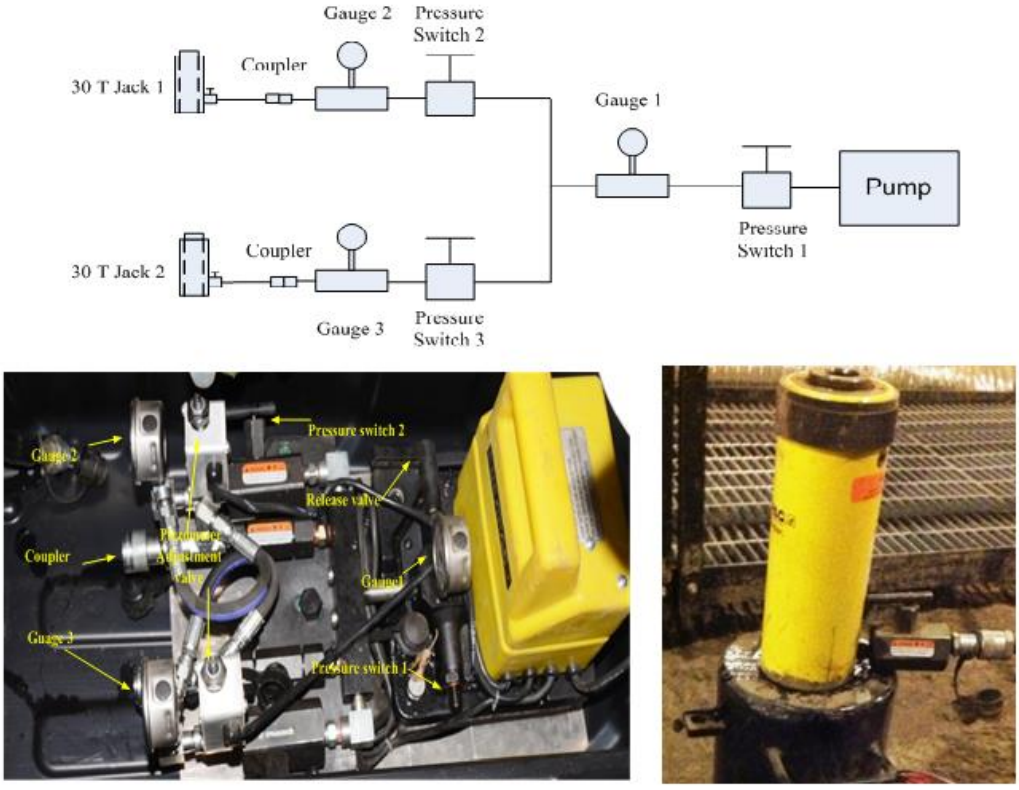

Figure 3.6 Hydraulic Pump System

3.2.2 Sensors

The HPI strain gage is used in the test to measure the strain in the anchor tendon as shown in Figure 3.7. This strain gage has four arm bridges, which ensure an outstanding stability and temperature compensation. The head of the strain gage consists of a precision foil gage unit

bonded to a stainless steel shim, an amplifier, and a voltage regulator. The two metal tabs that extend from part of the gage head are used to attach the gage to the anchor tendon.

Figure 3.7 HPI Full Bridge Weldable Strain Gage

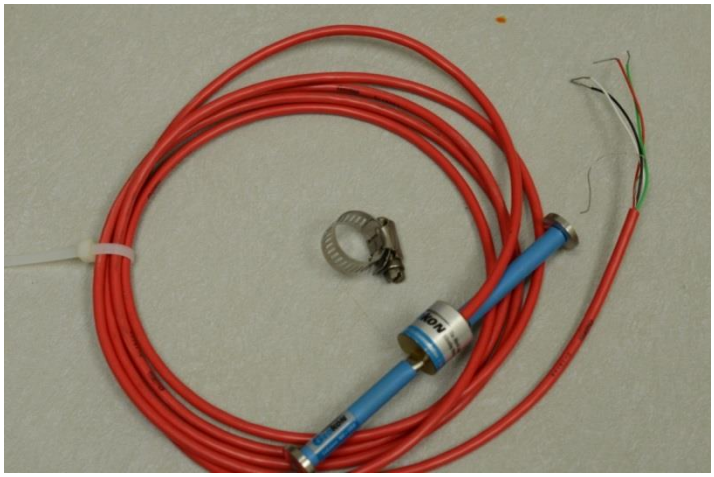

Figure 3.8 Geokon M4200 Strain Gage

As shown in Figure 3.8, Geokon Model 4200 vibrating wire strain gage is designed for long-term strain measurements in mass concrete and structures such as foundations, piles, bridges and dams. Vibrating wire strain gage has excellent long-term stability, maximum resistance to the effect of water and an output frequency suitable for transmission over very long cables.

An LVDT is used to measure the displacement of the anchor, as shown in Figure 3.9. This device produces an output voltage proportional to the mechanical displacement and contains three coils;

one primary coil and two secondary coils. The primary coil is where the converted DC voltage is applied. One of the secondary coils generates a corresponding voltage to the change of position of magnetic core, and the other one generates zero voltage for the output.

Figure 3.9 Omega LD600-25 LVDT

3.2.3 Data Acquisition System

All test data is automatically recorded by the CR1000 data logger, as shown in Figure 3.10. The data acquisition system consists of one CR1000 control panel, two AM16/32 relay multiplexers, and one AVW200 vibrating wire interface. The function of each instrument is described as follows: The CR1000 provides a 12 V output power to the multiplexers and AVW200, and 5 V output power to the two LVDTs. The CR1000 records all data from the multiplexers and analyzes that data according to a program contained in the CR1000. Multiplexers provides the many data channels needed for a single data logger to simultaneously record data from many sensors. Without multiplexing capability, only four HPI or Geokon strain gages can be connected to one CR1000 data logger. With the two AM16/32 multiplexers, it is possible to obtain data from as many as 32 HPI or Geokon sensors. The AVW200 vibrating wire interface is needed to allow the data logger to read the data signal from the Geokon vibrating wire sensors.

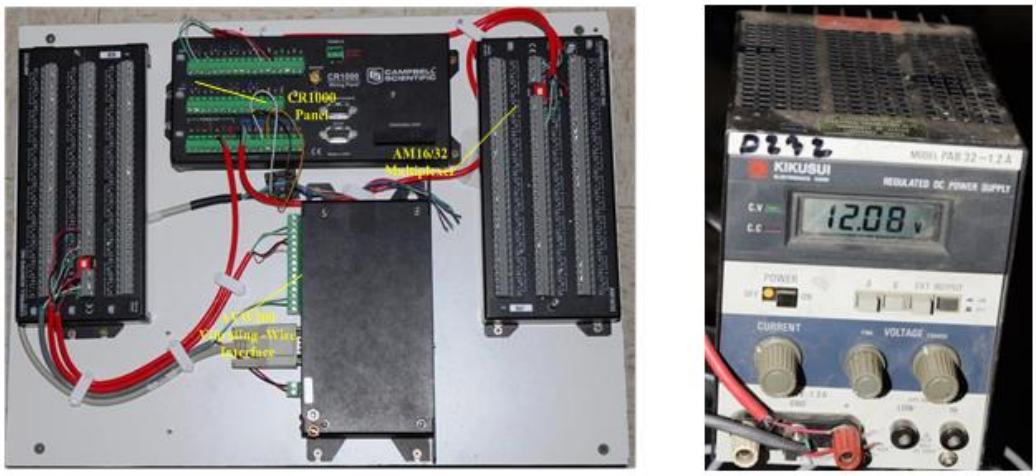

Figure 3.10 Data Acquisition System

3.3 TEST PREPARATION

3.3.1 Drilling Boreholes

The diameters of the boreholes are 4.0 in (101.6 mm) for grouted anchors and 2.0 in (50.8 mm) for duckbill anchors. The depths are 10.0 ft (3.0 m) for grouted anchors and 6 ft (1.8 m) for duckbill anchors. Figure 3.11 gives the layout of the drilling system. The drilling system consists of a drilling machine, circulating fluid, and power supply. The drilling machine used in the permafrost tunnel is a Model MP260 manufactured by the TEI Rock Drill Company. The MP260 is a portable, two-wheeled, hydraulically powered drill that weighs about 450 lbs (205 kg). The drill is powered by a diesel power unit located outside the tunnel, to the right side of the entrance. And the air compressor locates on the left side of the entrance provides compressed air as circulating fluid. The hydraulic oil tubes and compressed air tube go into the tunnel through a hole opened on the right side of the tunnel entrance. Hydraulic lines transfer power from the power unit to the drill. An air compressor is located outside and to the left of the entrance. The compressor provides compressed air to the vicinity of the drill bit that keeps the borehole blown free of loose chunks of material.

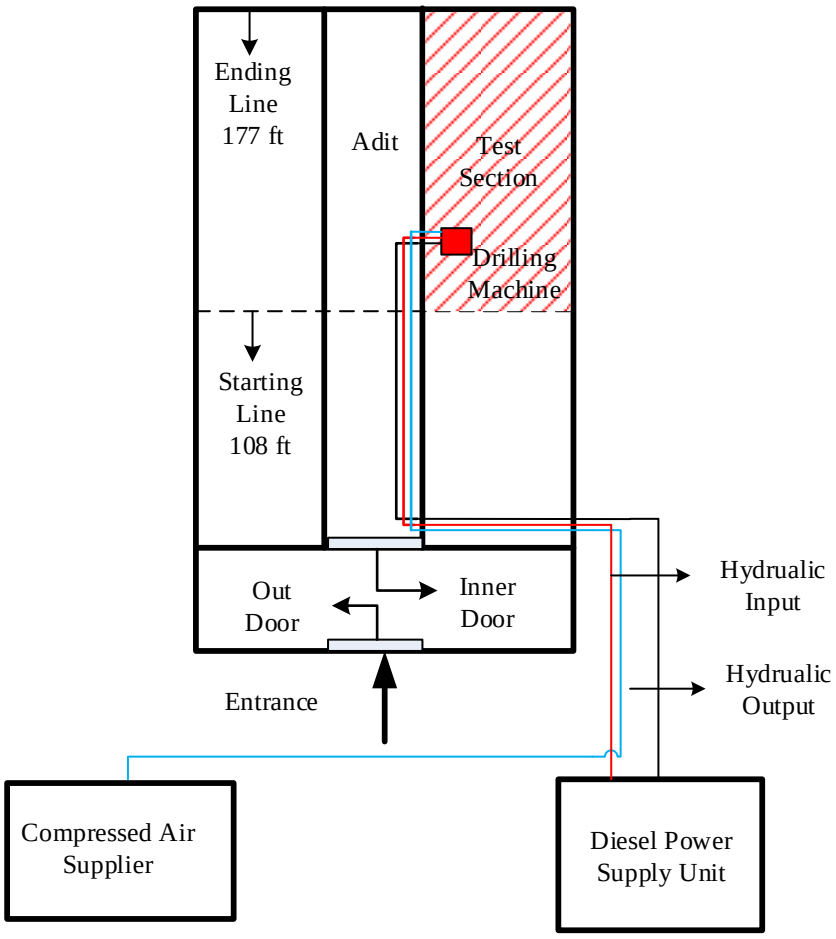

Figure 3.11 Drilling System Layout

Figure 3.12 shows detailed information of the setup process of the drilling machine. The drilling process started with the boreholes on the left side of the test zone, closer to the main adit. When the drill was in place for each hole, a rod (which had been welded to the top of the drill) was wedged against the tunnel ceiling to prevent the drilling machine from shaking back and forth or moving vertically. At the bottom of the drill were two leveling screws, used to plumb the drill. Three lines were connected to the drill head: two were hydraulic lines that provided drilling power, and one was a compressed air line for keeping the hole clear.

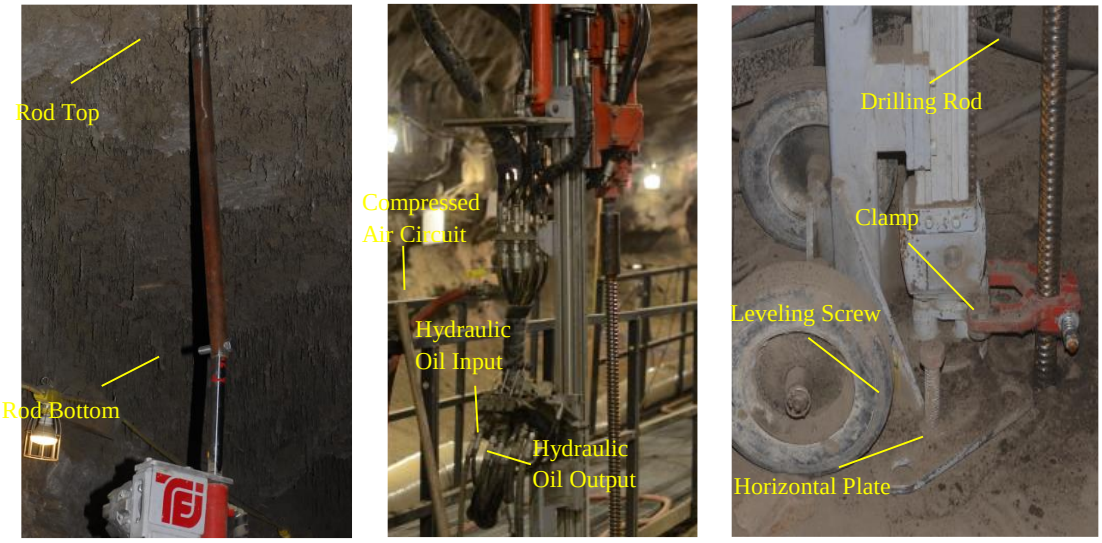

(a) (b) (c)

Figure 3.12 Drilling Machine Setup Procedures

After setup, the drilling process began, as shown in Figure 3.13. One end of a 5 ft (1.67 m) drill rod was connected to the drill head with a coupling device, and the drill bit was attached to the other end of the drill rod. At the start of the drilling process, the driller's assistant gripped the drill rod and placed the drill bit at the exact spot to begin drilling. The driller then advanced the drill bit into the soil 2-4 in (51-101 mm), and stopped to hook the stabilizing clamp, located near the bottom of the drill, around the drill rod. Compressed air was blown down the borehole through the hollow drill rod during the drilling process to prevent loose material from blocking the hole. After every 1-2 ft (0.33-0.66 m) of drill bit advance, the drill head was moved up and down several times to refine the shape of the borehole and bring the soil cuttings to the ground surface. After the bit reached a depth of about 4.5 ft (1.5 m), the top of the drill rod was detached from the drill head and another 5 ft (1.67 m) length of drill rod was coupled to the first drill rod. The top of the second rod was then connected to the drill head, and the drilling process continued to a final depth of 10 ft (3.33 m). After reaching the target depth, the drill rod was removed from the borehole. As Figure 4.19(d) shows, the 5 ft (1.67 m) lengths of drill rod were unscrewed for decoupling. During the decoupling process, it was necessary to attach a collar device to the top of the lower rod to keep it from dropping back into the borehole (such devices are often referred to as a "crow's foot").

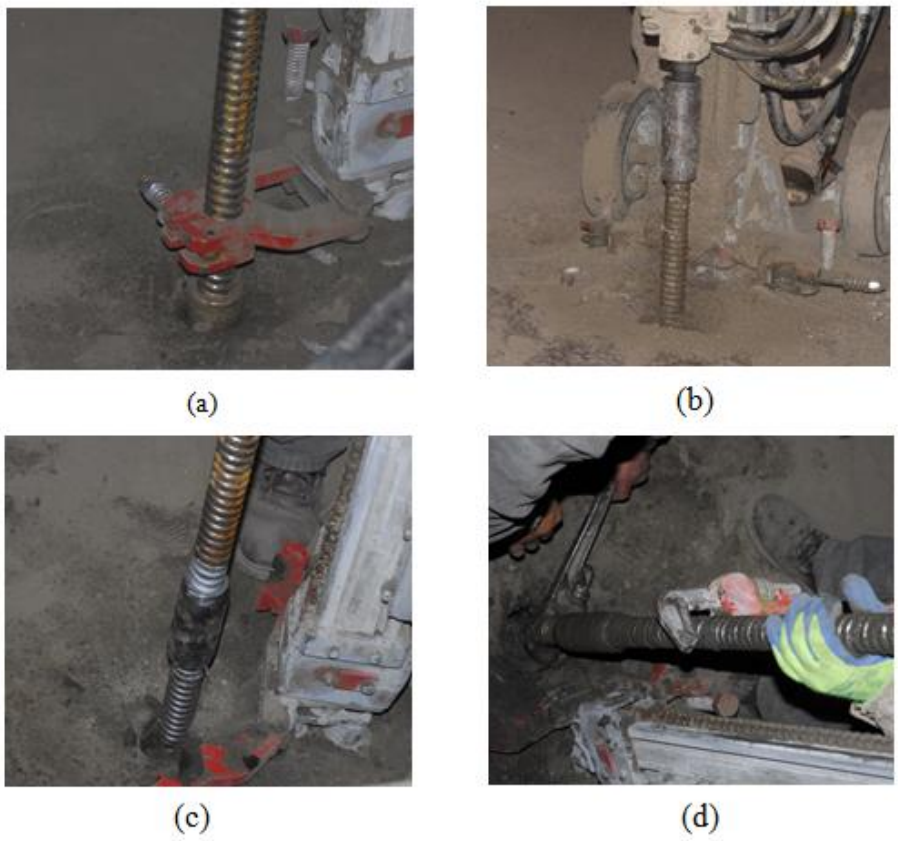

Figure 3.13 Borehole Drilling Procedures

3.3.2 Sensor Installation

The configurations of the shallow anchors are shown in Figure 3.14. The Geokon strain gages (yellow marks) were instrumented distributed along the anchor with an equal interval of 1.67 ft, starting at 1.50 ft (0.46 m) from the top and ending at 1.50 ft (0.46 m) from the bottom. The HPI strain gages (red marks) were installed at the same place, but were welded on the anchor tendon. At depths of 3.83 ft (1.17 m) and 6.16 ft (1.88 m), both sides of the anchor tendon were welded with HPI strain gages as indicators of the eccentricity of the applied load. In total, two types of anchor tendons are used in the field test: solid tendon and hollow tendon. The diameter of the solid tendon is 1.4 in (36 mm), and the outer and inner diameter of the hollow tendon are 1.6 in (40 mm) and 0.8 in (20 mm), respectively.

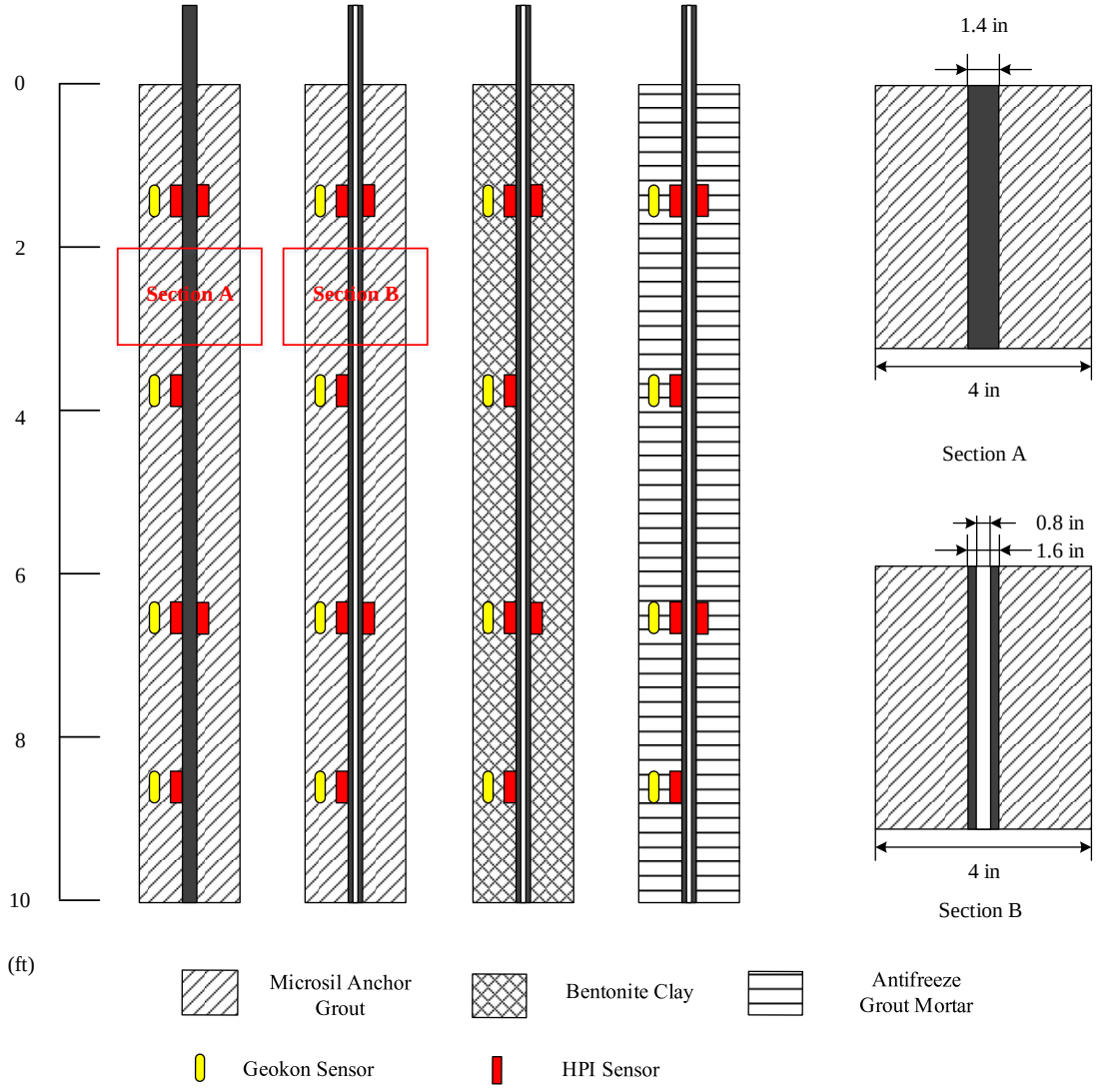

Figure 3.14 Grouted Anchors Configurations

Figure 3.15 shows the HPI strain gage installation process. After the anchor tendons were properly prepared, the HPI sensors were attached by welding them in place on the anchor bars. A Sunstone D-CD320 spot welder was used to weld the gages in place. The welding process first required welding the wings (attached to part of the sensor head) to the tendon. It was necessary to make sure that the sensor heads were positioned exactly at the center of the prepared areas on the bars. One spot weld at the center of each wing initially affixed the wing to the bar. Following initial attachment of the wing, additional spot welds were added to ensure attachment that would survive the anchor testing process. Next, the rectangular gaging unit itself was carefully attached to the tendon with several spot welds. All spot welding was done using specific patterns of weld

placement to prevent damage to the gage components while achieving a high-strength attachment. During the spot welding process, welds at certain locations along the margin of the gage could not be too close to the gage's critical components. The critical strain sensing components were encased in stiff plastic and could be easily damaged by excessive heating caused by an improper welding technique.

(a) (b)

Figure 3.15 HPI Strain Gage Installation

Figure 3.16 gives the Geokon strain gage installation process. The Geokon strain gages and cables were loosely attached along the outside of the anchor bars using polyethylene zip-ties. Care was taken to avoid applying large forces to the end blocks of the sensors. The zip-ties were adjusted loosely to facilitate relative movement between the anchor tendon, the Geokon gages, and the cables during placement of the grout. Such movement was necessary to prevent damage to the sensor components. The sensor assemblies were protected from damage that could be caused by the vibration needed to densify the grout during placement. A strip of foam was wrapped between the sensor and tendon (see beneath the zip-ties). This foam layer provided a cushion between the zip-ties and the anchor tendon so that the vibration characteristics of the wire in the strain gage would not be affected by the ties. It was concerned that, without the foam cushion, overly tight zip-ties might influence the resonant frequency of the vibrating gage wire.

Such an effect might have resulted in unstable readings or no readings at all. After the zip-ties were cinched in place, the vibration actuator coil was affixed to the gage body with a hose.

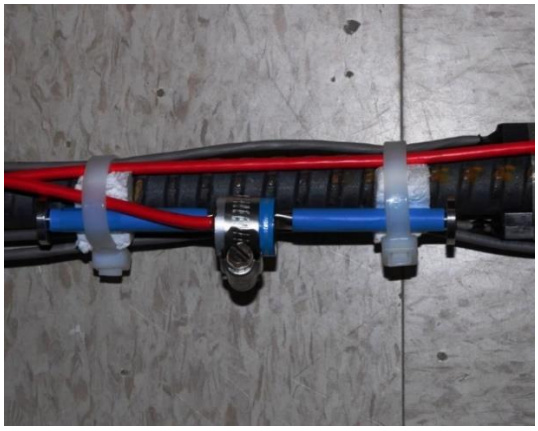

Figure 3.16 Geokon Strain Gage Installation

Following installation of all the HPI and Geokon sensors, the last step in preparing the anchor tendon was to attach a "centralizer" to the tendon. One centralizer device was wired to each anchor 5 in (127 mm) from the bottom to ensure that the tendon remained in the center of the hole during the grouting. Centralizers were simple devices made from short sections of PVC pipe, as shown in Figure 3.17. Some of the centralizers used on the solid anchor bars had to be modified to allow for passage of the grout tube to the bottom of the anchor. Grout was delivered to the bottom of the hollow tendon through the center of the bars, so no centralizer modifications were required.

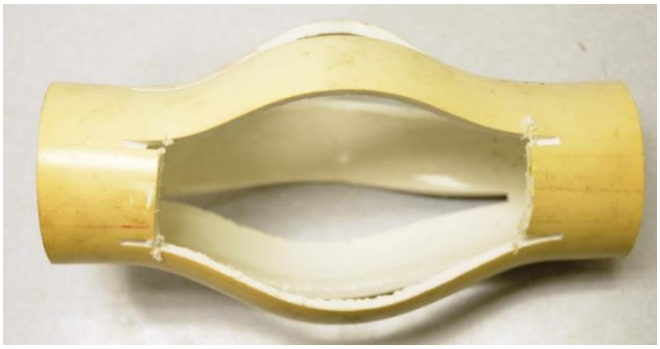

Figure 3.17 Centralizer

The instrumented anchor tendon assemblies were prepared at a location away from the dusty, cold permafrost tunnel. Final installation of the anchor tendon was a simple matter. The tendon

assemblies were transported to the permafrost tunnel, and each was placed into its respective borehole. Anchor rod assemblies were handled very carefully at all times prior to being inserted into the borehole in permafrost tunnel.

Insertion of the anchor bar assembly into the borehole required two workers, as shown in Figure 3.18a. The anchor was carefully lowered into the borehole to prevent the sensors from contacting the wall of the borehole. While one person lowered the anchor into the borehole, the other handled/fed instrumentation wires to assist the insertion. After insertion of each tendon, a piece of cloth was placed at the top of the borehole to prevent debris from entering the hole.

(a) (b)

Figure 3.18 Anchor Installation

3.3.3 Grouting Material

Three types of grouting materials were used: Microsil Anchor Grout, Bentonite Clay, and Antifreeze Grout Mortar. The Microsil Anchor Grout, manufactured by a Canadian Company, is an unsanded Portland cement-based, expanding grout containing silica fume, fly ash, and other additives. This type of backfill material gains strength quickly and resists water washout, which is ideal for anchors in a soil media. Moreover, this backfill material achieves excellent physical properties during curing at temperature down to 41°F (5°C) and exhibits freeze/thaw durability. The recommended water to cement ratio is 0.27 for a pumpable consistency and 0.31 for a

flowable consistency. The Bentonite Clay is a non-shrink, thermally-conductive Bentonite Clay provided by TCC Materials. The formulation is made with bentonite clay and silica sand with no hydration heat. The recommended water to clay ratio is 1.0 and the water needs to be heated to 32 °C before mixing. The Antifreeze Grout Mortar contains four types of chemical admixtures, including one accelerator, one corrosion inhibitor with slight acceleration properties, one mid-range water reducer and one high-range water reducer. The aim of this innovative grout mortar is to achieve three primary objectives: depress the freezing point of the mix water available for the hydration process, accelerate the early-age strength gain at low temperature, and enhance excellent flowability for grouting, tests such as flow, early-age strength, freezing point of the mix water, and setting time of mixes were selected (Lin et al., 2015).

The volume of the grouting material for one borehole was determined by the following equation:

$$V = R * \frac{\pi}{4} * D^2 * H * 12 \tag{3.1}$$

where V is volume (in^3), R is the redundancy factor (R=1.3), D is diameter of the borehole (D=4.0 in), and H is the depth of the borehole (H=10 ft).

The equipment used for mixing the grouting material is shown in Figure 3.19. Inside the container were three sets of impeller blades (at bottom, middle, and top of container) that stirred and blended the grout mixture. After sufficient mixing, the grout mixture was released from the grout-mixing tank through a valve at the bottom of the tank.

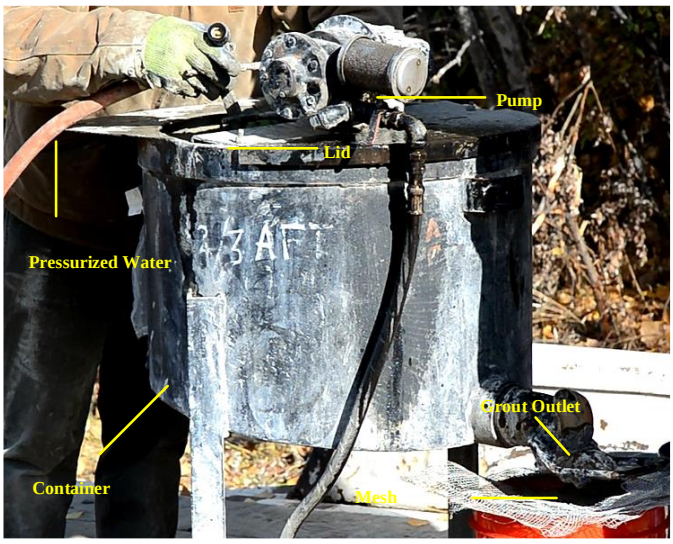

Figure 3.19 Grouting Material Mixing Equipment

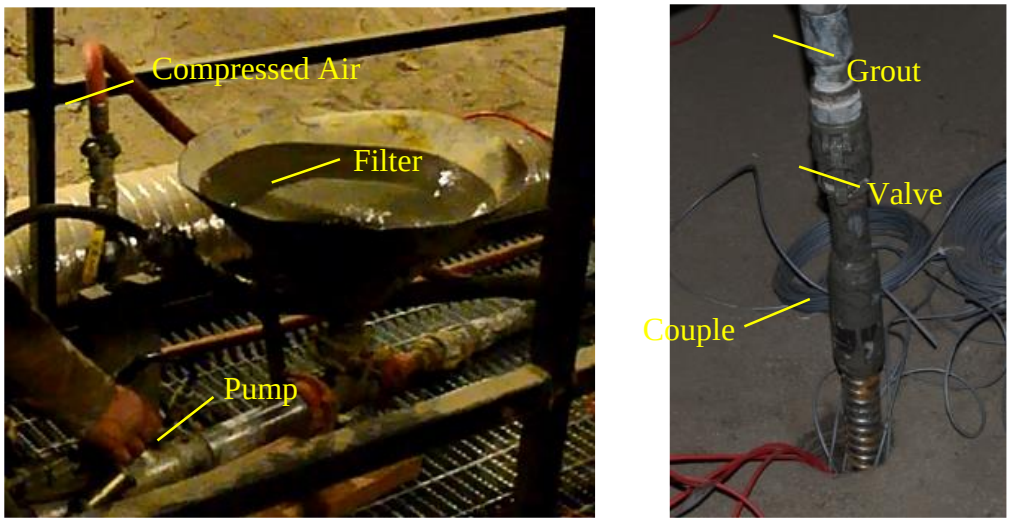

(a) (b)

Figure 3.20 Grouting Equipment and Connection

High-pressure grout pumping equipment was used to completely pump the grout to completely fill the annulus between the borehole walls and the anchor tendon. The grouting equipment used in the permafrost tunnel is shown in Figure 3.20. After mixing, the grout was carried into the tunnel by workers and poured into the grout pump's hopper. From the hopper the grout was gravity-fed into the pump unit, where it was pressurized and then delivered through a grout tube to the base of the anchor tendon, thereby filling the borehole annulus from the bottom up.

After the borehole had been fully grouted, it was necessary to hold the top of the anchor for several minutes so that the grout could set enough for the steel bar to remain stable in the center of the borehole. A successfully grouted anchor is shown in Figure 3.21.

Figure 3.21 Anchor after Installation

3.4 TESTING PROCEDURE

3.4.1 Duckbill Anchor

Before testing the duckbill anchors, tension strength tests had been conducted in the lab in order to determine the ultimate strength of the duckbill cable. The ultimate strengths of the tested three cables were quite consistent, between 1690 lbs (6.0 KN) and 1760 lbs (7.8 KN), and the total displacements for the three cables ranged from 0.33 in to 0.54 in (8.40 mm to 13.70 mm). Even though the cable displacement depended on the total length of the cable, which might vary from one to another, the slopes of the curves were at the same magnitude (0.00012 in/lb).

During the field tests, only one of the duckbill anchors (Anchor 13) was successfully installed in the normal way (set with a jack load). After numerous attempts at normal installation, the three remaining duckbill anchors were inserted into their respective boreholes, and a gravel backfill material was placed into the hole, followed by enough water to fill the voids in the gravel. This installation method created a 6 ft long, frozen gravel “plug” above the head of the duckbill anchor. The freeze-back time for the saturated gravel was relatively short, less than 2 days. Plus, Long-term creep tests were performed on anchors 13 and 17 for one month at load level of 1320 lbs (6 KN). Table 3.2 gives the loading schedule for all 4 duckbill anchors.

Table 3.2 Loading Schedule for Duckbill Anchors

Anchor No.	Loading Schedule (lbs)					Short-Term or Long-Term
	1	2	3	4	5	
13	440	660	880	1100	1320	Long-Term
14	440	660	880	1100	1320	Short-Term
16	440	660	880	1100	1320	Short-Term
17	440	660	880	1100	1320	Long-Term

3.4.2 Grouted Anchor

Two types of tests were conducted on the 13 grouted anchors, including creep test and pullout test. The temperature changes for each anchor were monitored for a period of 7 days.

For creep test, anchor 1 and 3 were loaded from 5 tons to 20 tons (50 KN to 200 KN) in order to have a general idea of the creep behavior of the anchors. And the results indicated that very limited creep deformation was observed at 5 tons (50 KN) and obvious creep deformation was observed at 20 tons (200 KN). Therefore, the rest of the anchors adopted a three-stages loading schedule, which were 7 tons (70 KN), 12 tons (120 KN) and 15 tons (150 KN). The detailed loading schedule is shown in Table 3.3.

The pullout test was conducted on August 28, 2013. The ultimate capacity of the anchor tendon was 60.6 tons (606 KN), so that no load above 55 tons (550 KN) shall be applied to the anchors just for safety concerns. Table 3.4 gives the loading schedule for the pullout test.

Table 3.3 Creep Test Loading Schedule

Anchor	Grouting Material	Loading Schedule (tons)
1	Microsil Anchor Grout (with Solid Tendon)	5, 10, 15, 20
2		7, 12, 15
3		5, 10, 15, 20
4		7, 12, 15
5	Microsil Anchor Grout (with Hollow Tendon)	7, 12, 15
6		7, 12, 15
7		7, 12, 15
8	Bentonite clay (with Hollow Tendon)	7, 12, 15
9		7, 12, 15
10		7, 12, 15
11	Antifreeze Grout Mortar (with Hollow Tendon)	7, 12, 15
12		7, 12, 15
15		7, 12, 15

Table 3.4 Pullout Test Loading Schedule

Anchor	Grouting Material	Loading Schedule (tons)
1	Microsil Anchor Grout (with Solid Tendon)	15, 30, 45, 55
2		15, 30, 45, 55
3		15, 30, 45, 55
4		15, 30, 45, 55
5	Microsil Anchor Grout (with Hollow Tendon)	15, 30, 45, 55
6		5, 10, 15, 20, 25, 30, 35, 40, 45, 50, 55
7		15, 30, 45, 55
8	Bentonite clay (with Hollow Tendon)	5, 10, 15, 20, 25, 30, 35, 40, 45, 50, 55
9		15, 30, 45, 55
10		15, 30, 45, 55
11	Antifreeze Grout Mortar (with Hollow Tendon)	15, 30, 45, 55
12		5, 10, 15, 20, 25, 30, 35, 40, 45, 50, 55
15		15, 30, 45, 55

CHAPTER 4 TEST RESULTS AND ANALYSES

In this chapter, both test results of duckbill anchors and grouted anchors are presented and discussed. First, the short-term and long-term creep results of duckbills are presented. Then, the comparison of the temperature changes of different grouting materials is made to analyze its effects on surrounding soils. The analysis of anchor creep test involves the load distribution along the anchor shaft and the displacement vs. time curves. Finally, the pullout test results are illustrated to give a better understanding of the pullout capacity of the anchor.

4.1 DUCKBILL ANCHORS TEST RESULTS AND DISCUSSIONS

As shown in Figures 4.1 and 4.2, both short-term and long-term test results indicated that the apparent creep behavior of the anchors was mainly generated by stretching of the duckbill cable. Total displacements measured at the ground surface for all of the duckbill anchors were acceptable.

Figure 4.1 shows the test results for two of the duckbill anchors. Both of the anchors experienced very limited displacement at each load level. The relatively instantaneous cable stretching was caused by the applied load increment. The slopes of the curves were nearly horizontal. The displacement slowly increased after load application by 0.11 in (2.70 mm) and 0.16 in (4.13 mm) for duckbill anchors 14 and 16, respectively, at the 1320 lbs (6 KN) load level. The cause of this relatively large displacement, significantly after placing the final load increment, is unknown. However, it is thought that it might have been due to breaking of cable strands as the total test load approached the ultimate strength of the cable. The total displacements for duckbill anchors 14 and 16 were 0.84 in (21.44 mm) and 0.85 in (21.60 mm), respectively.

Figure 4.2 shows the final testing results for duckbill anchors 13 and 17. At the starting load level, both of the anchors seemed to experience large, rapid displacements compared with duckbill anchors 14 and 16. For these two tests, the load frames themselves moved due to their unintentional placement on soft silt material covering the floor of the tunnel. The initial movement occurred only during the first 20 minutes. After the first 20 minutes, the displacements were more similar to those seen for duckbill anchors 14 and 16. Figure 4.2 contains two sets of lines for duckbill anchors 13 and 17. One set of lines plots the original data. The second (revised) set of lines is for corrected data from which the initial effect of load frame

movement has been subtracted. After revision, the total displacements for duckbill anchors 13 and 17 were 0.85 in (21.59 mm) and 1.11 in (28.28 mm), respectively. As mentioned previously, duckbill anchor 13 was the only duckbill anchor installed without gravel backfill. Therefore, a larger displacement for duckbill anchor 13 is reasonable due to the longer (completely unbounded) length of the cable and possible opening of the duckbill.

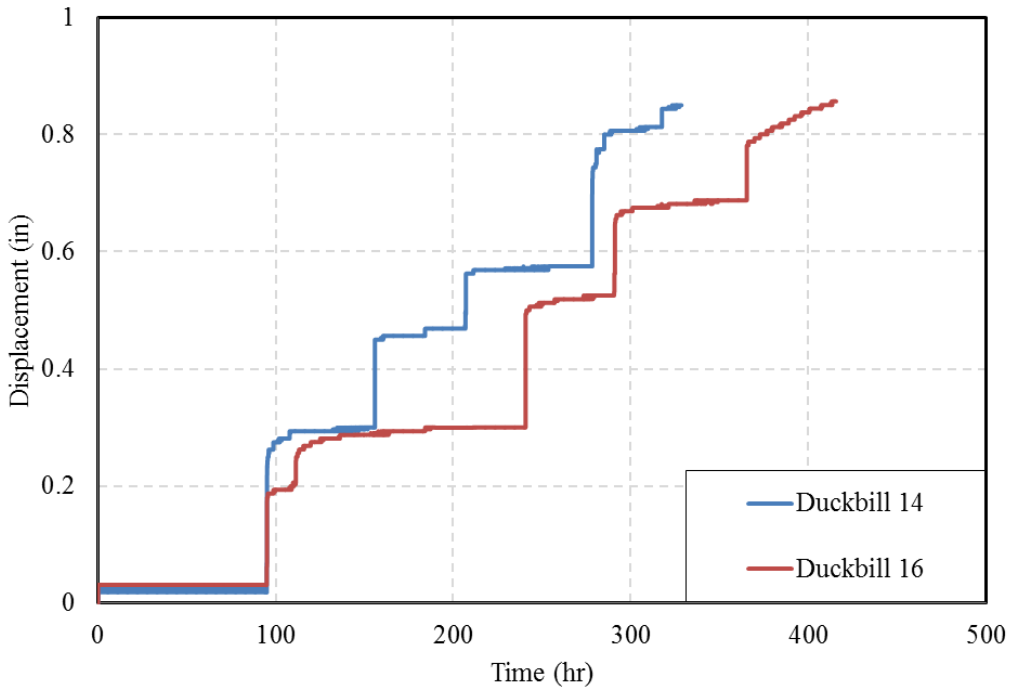

Figure 4.1 Displacement vs. Time for Duckbill Anchors 14 and 16 (Short-Term Test)

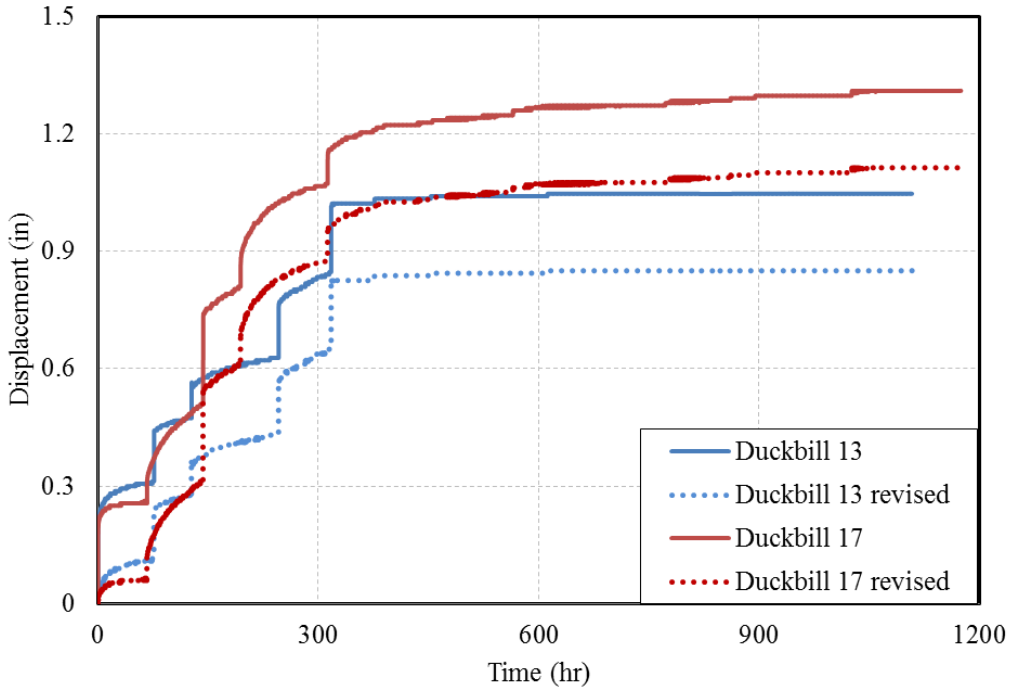

Figure 4.2 Displacement vs. Time for Duckbill Anchors 13 and 17 (Long-Term Test)

The long-term creep test results for duckbill anchor 17 was consistent with those of duckbill anchors 14 and 16. The total displacement at the 1320 lbs (6 KN) load level was 0.027 in (0.69 mm) for the long-term test, which is very limited and can be considered essentially no creep. Even for duckbill anchor 13, with its effectively longer anchor cable, the total displacement at this load level was only 0.138 in (3.50 mm), an amount considered tolerable.

In a summary, both the short-term and the long-term creep test results indicated that the total displacement of duckbill anchors with a load of 1320 lbs (6 KN) or less was limited to an acceptable range. Due to the difficulties encountered in installing three of the four duckbill anchors in permafrost, and the longer total displacement noted for the properly installed duckbill anchor, a modified installation method is recommended. It is suggested that duckbill in permafrost soils should be installed by inserting the duckbill anchor in a predrilled hole (of minimal diameter to allow anchor insertion), and backfilling the hole with saturated gravel or other locally available, similarly workable material. An incidental benefit of such installation should minimize cable stretch, especially for short-term loads as long as the cable retains its original “bond length” within the frozen backfill material.

4.2 GROUTING TEMPERATURE TEST RESULTS AND DICUSSIONS

During the grouting procedure, the grouting temperatures at different locations along the anchor were monitored for 7 days. The sensors 1-4 represent the temperature records of Geokon sensors at 1.5 ft, 3.83 ft, 6.16 ft and 8.5 ft (0.46 m, 1.17 m, 1.88 m and 2.59 m) from the bottom of the anchor, respectively.

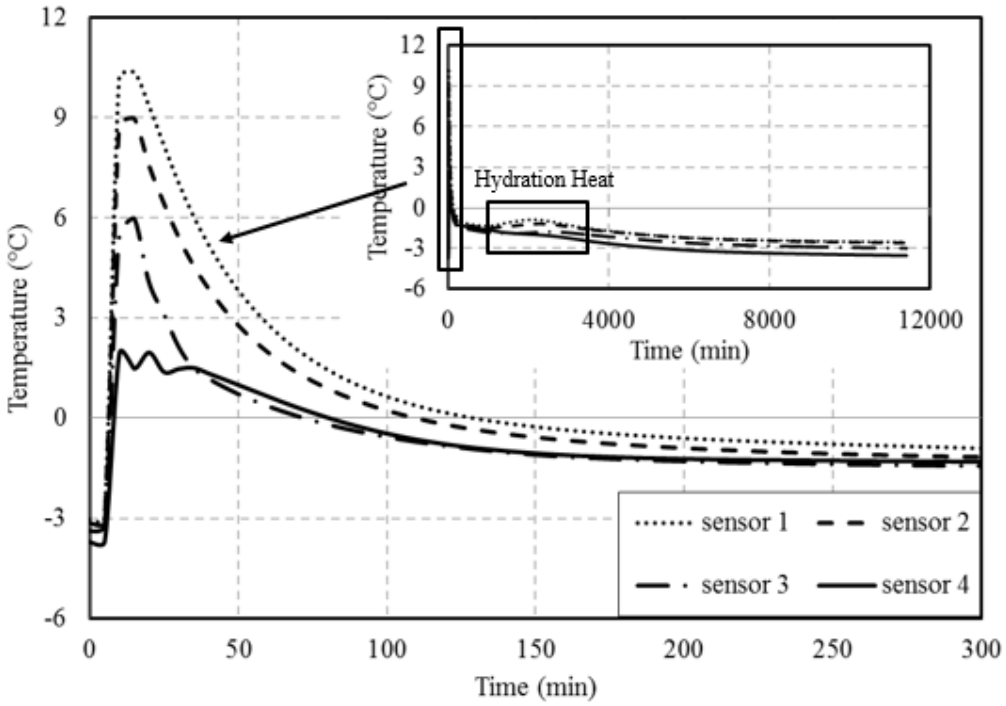

Figure 4.3 Temperature vs. Time for Anchor 2
(Solid Tendon with Microsil Anchor Grout)

Figure 4.3 gives the temperature vs. time curves for anchor 2, which is solid tendon grouted with Microsil Anchor Grout. The figure shows that the initial temperatures from bottom to top were about 25.3°F (-3.7°C), 25.9°F (-3.4°C), 26.4°F (-3.1°C), and 26.6°F (-3.0°C). The figure indicates that the temperature for the sensors at the top had almost returned to the initial temperature (the temperature surrounding the soil before grouting materials were poured into the borehole) after 5.6 days, while the temperature for the sensor at the bottom took longer time to freeze back. One can determine the duration of the grouting process by looking at the difference at the starting point of temperature change for different sensors. The grouting duration for anchor

was about 5 minutes. The smaller figure at the right upper corner of Figure 4.3 shows that the maximum temperature rise due to the hydration process was about 0.54°F (0.3°C).

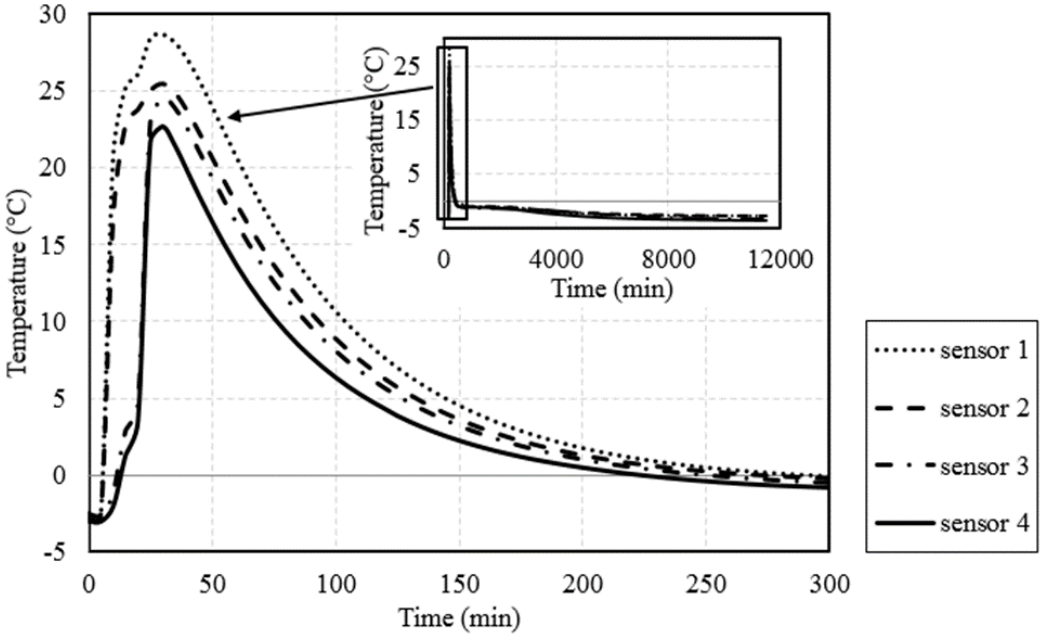

Figure 4.4 Temperature vs. Time for Anchor 8
(Hollow Tendon with Bentonite Clay)

Figure 4.4 shows the temperature vs. time curves for anchor 8, which is hollow anchor tendon grouted with Bentonite Clay. One sees that the initial temperatures for anchor 8 at different depths were almost the same (27.3°F), and the time for the grouting process for anchor 8 was less than 5 minutes. Moreover, the duration of temperature above 32°F for Bentonite Clay was much longer compared with other grout materials. This phenomenon might be caused by the high temperature of the mixing water, which was 90°F (32.2°C). The high temperature causes more thawing of the surrounding frozen soils, which should take a longer time to freeze back. Yet, the total time to freeze back for anchors with bentonite clay was shorter compared with anchors with Microsil Anchor Grout. Part of the reason might be that the hydration process, and therefore the output of hydration heat, for Microsil Anchor Grout lasted for a long time. On the other hand, use of the Bentonite Clay involved no hydration process and, therefore, no heat of hydration.

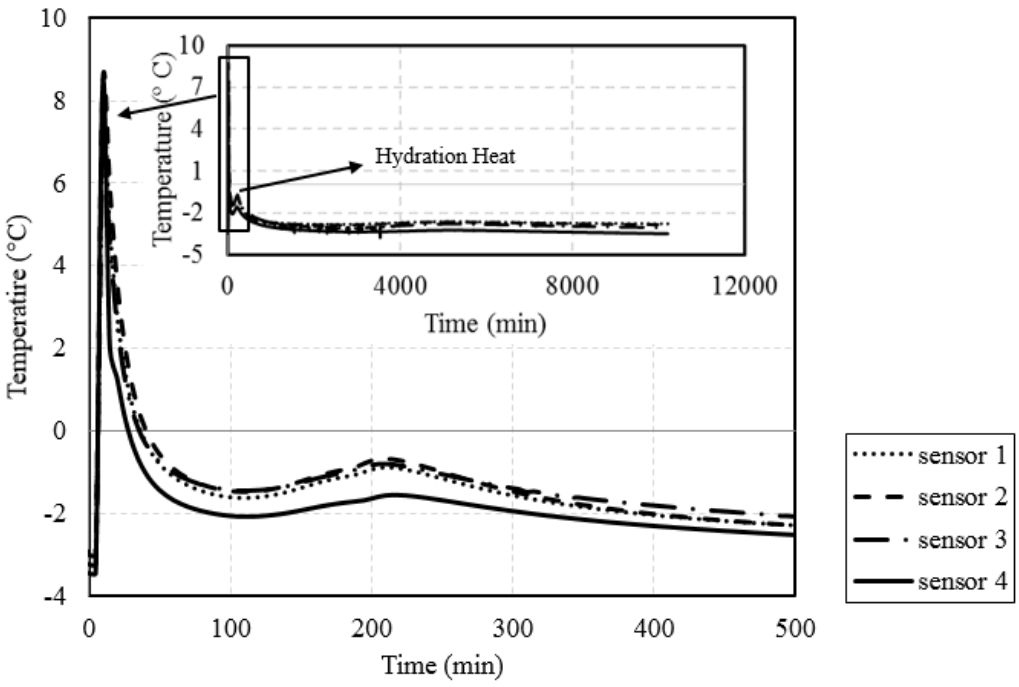

Figure 4.5 Temperature vs. Time for Anchor 11
(Hollow Tendon with Antifreeze Grout Mortar)

Figure 4.5 is the temperature vs. time curves for anchor 11 which is hollow tendon grouted with Antifreeze Grout Mortar. The highest temperature experienced was 47.3 °F (8.4°C). During the whole process, the heat generated from hydration process was lower than anchor 2 and the time to freeze back to initial temperature was also shorter, 2.8 days. And from Figure 4.5, a small amount of hydration heat generated increased the temperature by approximately 0.9°F (0.5°C). The time period for temperature above freezing point for Anchor 11 was only 5 hours. This relatively short time of reaction time would decrease the disturbance of the surrounding soil and also reduce the time to drop back to initial temperature.

In a summary, Figure 4.6 demonstrates the temperature changes for different grouts for the first 5 hours after grouting process completed. It was used to evaluate the permafrost degradation induced by hydration heat. Both the maximum temperature and the time lag for temperature above 0 °C can be served as indicators of the permafrost degradation. The monitored temperature was located at 3.83 ft (1.17 m) from the bottom of the anchor where the influence of the ambient environment on the temperature change could be neglected. In general, the average maximum

temperature were 44.4°F (6.9°C) for Microsil Anchor Grout, 76.3°F (24.6°C) for Bentonite Clay and 43.7°F (6.5°C) for Antifreeze Grout Mortar. Bentonite clay had the highest maximum temperature due to the warmer water (90°F or 32.2°C) used in the mixing procedure. And also, the total temperature increment were 18.4 °F (10.2°C), 49.5 °F (27.5°C) and 14.6 °F (9.7°C) for Microsil Anchor Grout, Bentonite Clay and Antifreeze Grout Mortar, respectively. Moreover, Bentonite Clay experienced the longest time lag (about 4 hours) with the temperature above 0°C indicating that it resulted in the largest permafrost degradation compared with the other two grouting materials (1 hour for Microsil Anchor Grout and 0.5 hour for Antifreeze Grout Mortar). Therefore the Antifreeze Grout Mortar had the least influence on the degradation of the surrounding permafrost.

Figure 4.7 is the temperature changes with different grouting materials for 7 days. It is used to evaluate the temperature increment resulted from hydration heat and the time lag needed for grouting materials to freeze-back to the initial temperature. Bentonite Clay did not experience temperature increase due to no hydration heat generated during the whole process. The time period for temperature freezing back to initial temperature was 5.5 days for Bentonite clay. The Antifreeze Grout Mortar experienced only about 0.9 days to freeze back to initial temperature and no obvious hydration heat was observed after 5 hours of the grouting process completed. The temperature increment induced by hydration heat for Microsil Anchor Grout was 0.9°F (0.5°C) and it also took about 5.6 days for the temperature freezing back to initial temperature, which was comparative with that for Bentonite Clay. In a summary, among all the three different backfill materials, Bentonite Clay provided the highest maximum temperature which would cause larger disturbance of the surrounding soil. Yet, the time to freeze back was shorter than that for Microsil Anchor Grout due to no extra heat generated after grouting. For Microsil Anchor Grout, even though the maximum temperature was not as high as Bentonite Clay, the heat generated by hydration increased the time for soil to freeze back. Finally, the Antifreeze Grout Mortar exhibited lower maximum temperature than that for Bentonite Clay. Meanwhile it took less time to freeze back to initial temperature than Microsil Anchor Grout. Therefore, Antifreeze Grout Mortar was more suitable for cold region applications.

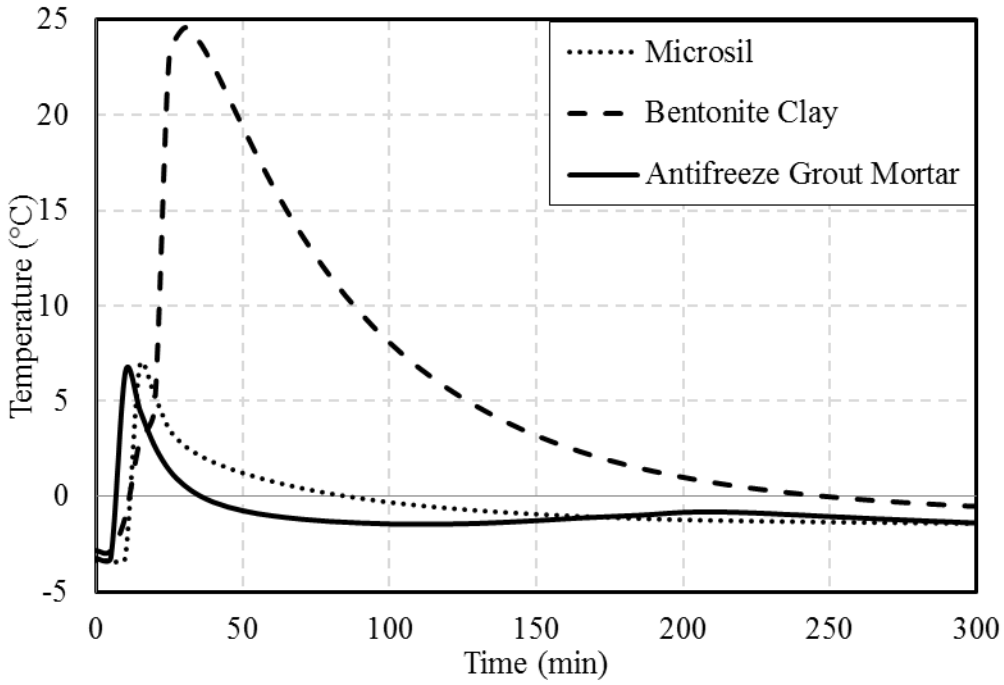

Figure 4.6 Temperature vs. Time for Different Grouting Materials (5 Hours)

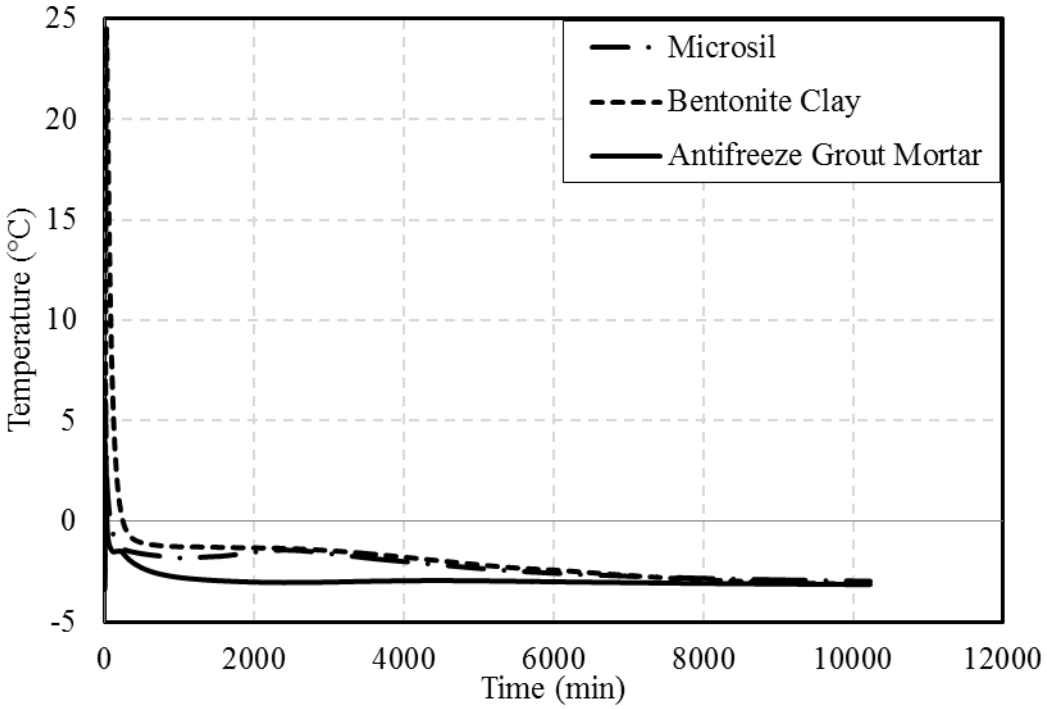

Figure 4.7 Temperature vs. Time for Different Grouting Materials (7 Days)

4.3 LOAD DISTRIBUTION RESULTS AND DISCUSSIONS

4.3.1 Theoretical Analysis of the Load Distribution along Anchor Shaft

There are several assumptions used in the analyses as follows:

1. Both tendon and grout behave in linear elastic pattern;
2. In radial direction, normal stress and strain are linearly distributed;
3. Grout only transfers shear stress due to the free top and bottom surfaces of the anchor;
4. Poisson's effects of all materials are neglected.

Figure 4.8 represents the free body diagram within any arbitrary anchor cross section. σ_r is the stress in tendon. σ_{ge} is the stress at interface of grout and soil, and σ_g is the stress at interface of grout and tendon. σ_u is the uniformly distributed stress related to σ_r. σ_o and σ_i are the decomposed stresses. D and B represent the diameter of tendon and anchor. R is the distance between neutral plane and longitudinal direction.

The stress in tendon, σ_r, was measured using the HPI strain gage. Since the Geokon strain gage in the grout is closer to the longitude axis, σ_g can also be determined by the measured strain in Geokon strain gage. The key point is to determine the stress at the edge of the grout, σ_{ge}.

Based on the above assumptions, the stress in grout is linearly distributed. The closer to the longitudinal axis, the larger the stress is. Using superposition method, the stress in the grout can be divided into two equivalent stresses, one is a constant stress, σ_u, and the other is linearly distributed with σ_L and σ_y, bending moment which can be expressed in terms of two normal stresses. The constant tensile stress, σ_u, could be determined by the force equilibrium of cross section area:

$$P = \sigma_u \pi \frac{(B^2 - D^2)}{4} + \pi \frac{D^2}{4} \sigma_r \tag{4.1}$$

where P is applied load; B is anchor diameter; D is anchor tendon diameter; σ_r is stress in anchor tendon; and σ_u is constant tensile stress.

Therefore, the constant tensile stress is given by Equation (4.2):

$$\sigma_u = \frac{4P - \pi D^2 \sigma_r}{\pi (B^2 - D^2)} \tag{4.2}$$

Because the strain is linearly distributed, the strain ratio of the outer edge and inner edge should be equal to their distance ratio to the neutral plane:

$$\frac{\sigma_o / E_g}{\sigma_i / E_g} = \frac{B/2 - R}{R - D/2} \tag{4.3}$$

Where σ_o is decomposed stress at the outer edge of the grout; σ_i is decomposed stress at the inner edge of the grout; E_g is Young's modulus of the grout; B is anchor diameter; D is anchor tendon diameter; and R is neutral plane.

The relationship between σ_o and σ_i thus can be expressed as:

$$\sigma_o = \frac{B - 2R}{2R - D}\sigma_i \tag{4.4}$$

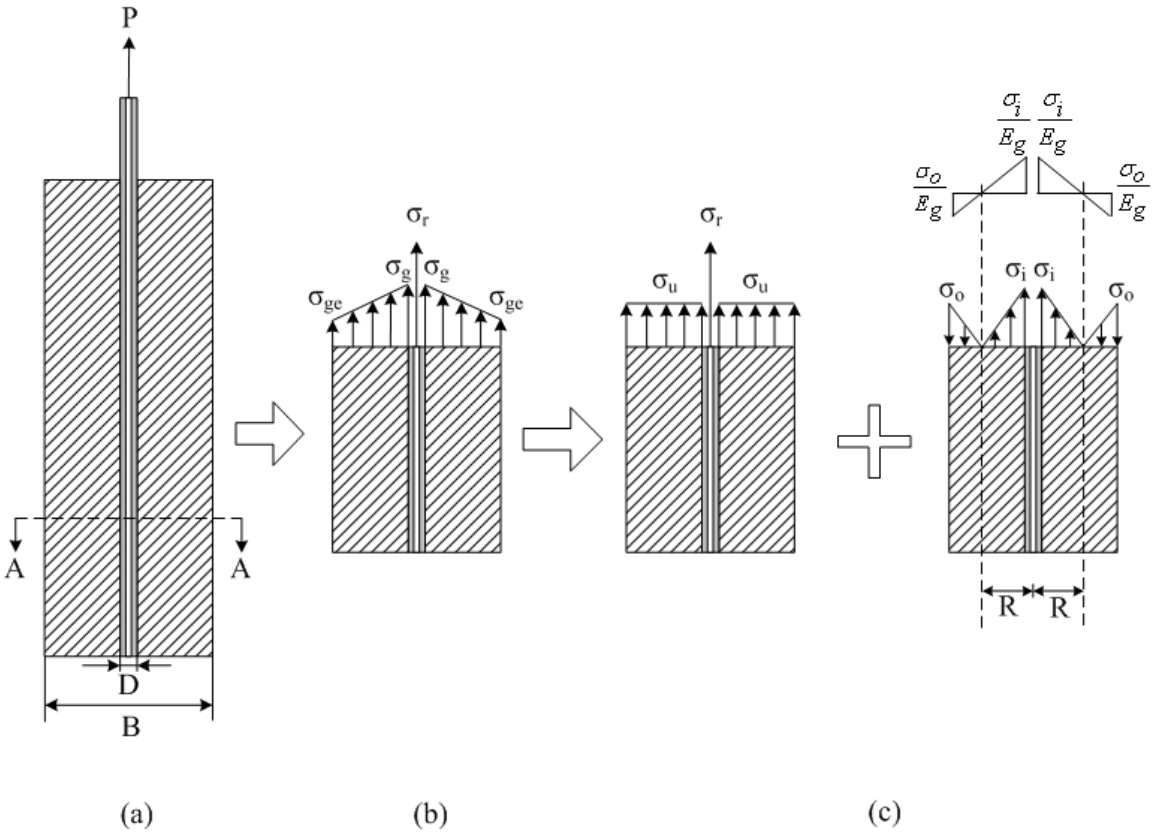

Figure 4.8 Free Body Diagram within Arbitrary Anchor Cross Section

The force equilibrium at the cross section area gives Equation (4.5), and Equation (4.6) represents the functions of decomposed stresses with respect of radius position, x:

$$\int_{\frac{D}{2}}^{R} \sigma_i dA = \int_{R}^{\frac{B}{2}} \sigma_o dA \tag{4.5}$$

$$\sigma_i(x) = -\frac{\sigma_i}{(R - D/2)}x + \frac{R\sigma_i}{(R - D/2)}$$

$$\sigma_o(x) = \frac{\sigma_o}{(B/2 - R)}x - \frac{R\sigma_o}{(B/2 - R)} \tag{4.6}$$

where σ_o is decomposed stress at the outer edge of the grout; σ_i is decomposed stress at the inner edge of the grout; A is effective area; B is anchor diameter; D is anchor tendon diameter; R is neutral plane; and x is radius position.

By solving Equation (4.5), the position of neutral plane can be determined as:

$$R = \frac{B^2 + BD + D^2}{3(B + D)} \tag{4.7}$$

There are two methods to represent the resultant moment within in the grout, as shown in Equation (4.8) and (4.9):

$$M_g = \int_{\frac{D}{2}}^{R} \sigma_i(x)(R - x)dA + \int_{R}^{\frac{B}{2}} \sigma_o(x)(x - R)dA \tag{4.8}$$

$$M_g = (P - \pi\frac{D^2}{4}\sigma_r)(R - \frac{D}{2}) \tag{4.9}$$

where σ_r is the stress in rebar; σ_o is decomposed stress at the outer edge of the grout; σ_i is decomposed stress at the inner edge of the grout; M_g is resultant moment; P is applied load; R is neutral plane; A is effective area; B is anchor diameter; D is anchor tendon diameter; and x is radius position.

By solving Equation (4.8) and (4.9), the relationship between σ_o (or σ_i) and σ_r can be determined. Moreover, σ_u can be written as a function of σ_r and the expression has been given by Equation (4.2).Therefore, stress at the inner edge of the grout σ_g , can be expressed as:

$$\sigma_g = \sigma_u + \sigma_i = [\frac{2P}{\pi(B - D)} - \frac{D^2\sigma_r}{2(B - D)}]M \tag{4.10}$$

where σ_r is the stress in rebar; σ_g is the stress in anchor tendon; σ_o is decomposed stress at the outer edge of the grout; σ_i is decomposed stress at the inner edge of the grout; P is applied load; B is anchor diameter; D is anchor tendon diameter; and M is constant value.

$$M = \frac{2}{B+D} + \frac{1}{\frac{D}{2}\left[\frac{(B-D)^2}{6(R-D/2)} - \frac{B-D}{R-D/2} + 2\right] + \frac{(B-D)^3}{16(R-D/2)^2} - \frac{(B-D)^2}{3(R-D/2)} + \frac{B-D}{2}}$$

Since σ_i is the only unknown variable in Equation (4.10), it can be determined and therefore σ_i could also be calculated by using Equation (4.4).

4.3.2 Load Distribution Test Results and Analysis

Figure 4.9-4.11 are the load distribution curves for anchors 3, 8 and 11, respectively. The dash and dot lines represent the load distribution in grout and anchor tendon. The solid lines stand for the load distribution in anchor. Also, the positive values indicate compressive strength and the negative values indicate tensile strength.

As shown in Figure 4.9, at low load level such as 5 tons (50 KN), for anchor at depth greater than 6 ft, the load in grout, anchor tendon, and anchors were all zero, indicating that the load did not transfer to the bottom of the anchor. At load level of 20 tons (200 KN), the grout experienced compression, which indicated that crack occurred and the location of the crack was at depths between 1.50 ft and 3.83 ft (0.46 m to 1.17 m). Moreover, at low load level (5 tons and 10 tons, or 50 KN and 100 KN), the upper part of the anchor sustained most of the applied load while at higher load level (15 tons and 20 tons, or 150 KN and 200 KN), the load gradually transferred to the lower part of the anchor.

Figure 4.10 shows the load distribution of anchor 8. Anchor 8 was made of a hollow anchor tendon with Bentonite Clay. At the moment the load was applied on the anchor, the crack occurred immediately. At load level of 15 tons (150 KN), crack occurred at both the bottom and upper part of the anchor. The bond between the tendon and grout only existed from 3 ft to 6 ft (0.9 m to 1.8 m). Therefore, the load was much larger in the middle part than the upper and lower parts.

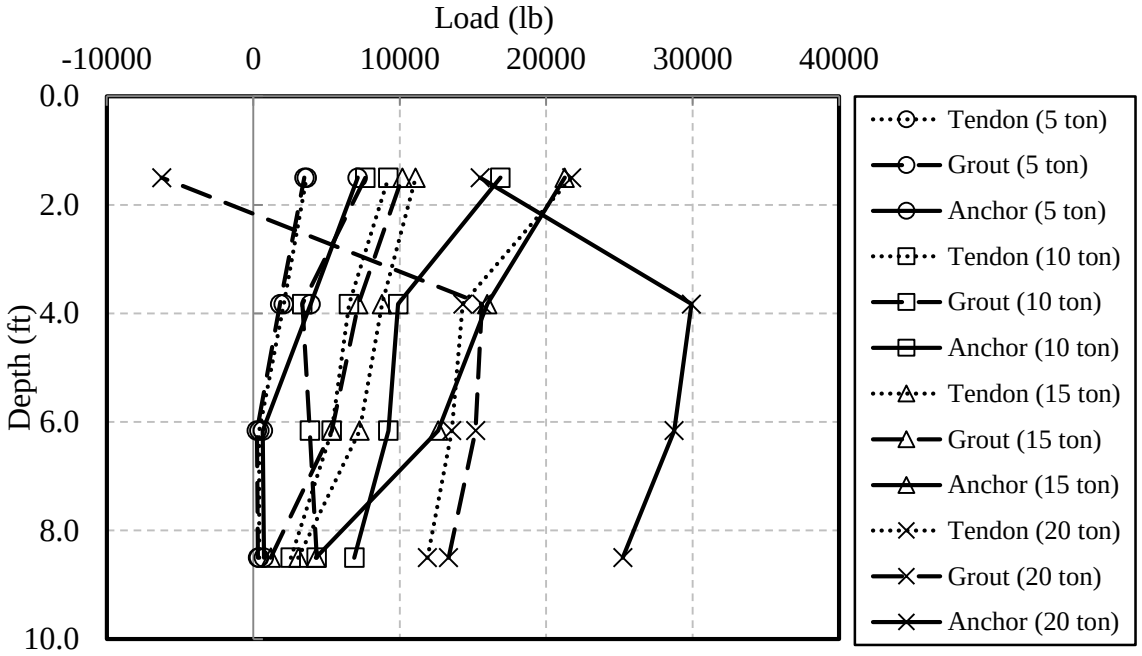

Figure 4.9 Load Distribution for Anchor Grouted with Microsil Anchor Grout (Anchor 3)

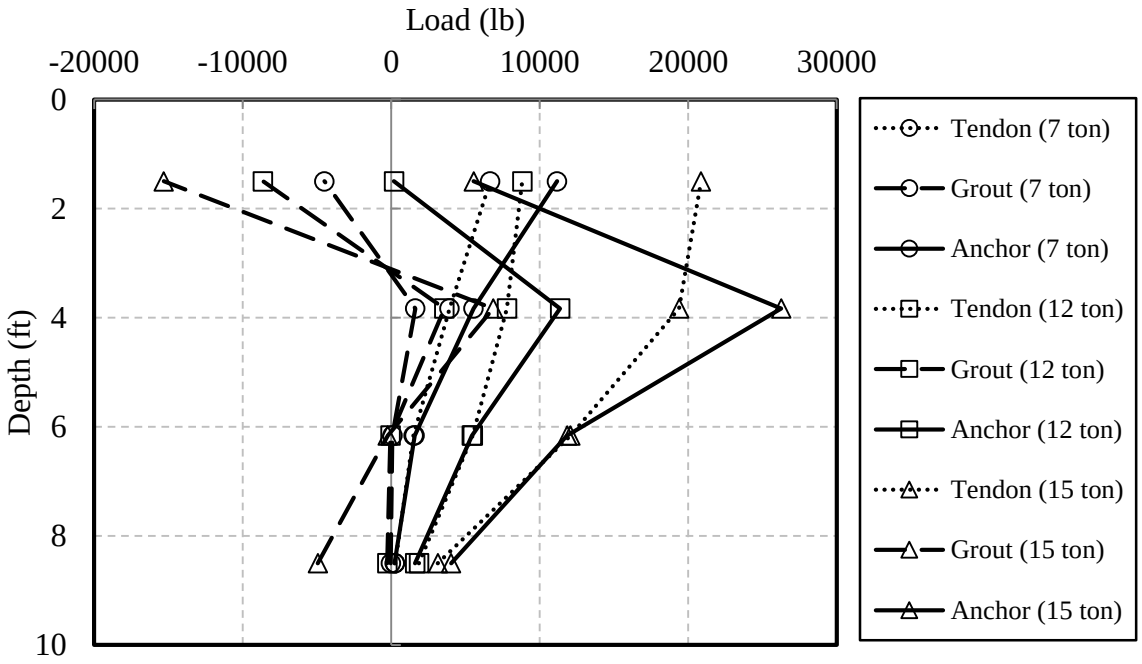

Figure 4.10 Load Distribution for Anchor Grouted with Bentonite Clay (Anchor 8)

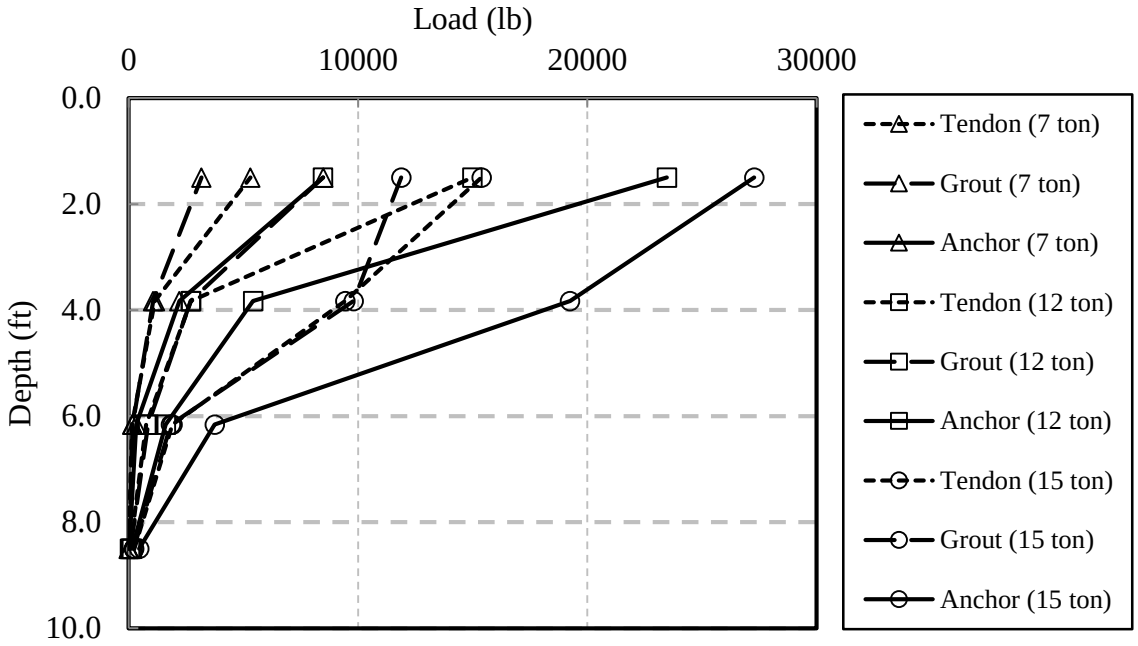

Figure 4.11 Load Distribution for Anchor Grouted with Antifreeze Grout Mortar (Anchor 11)

Figure 4.11 shows the load distribution curves for anchor 11 Anchor 11 consisted of a hollow anchor tendon grouted with Antifreeze Grout Mortar. Different from anchors 3 and 8, no crack was observed during the loading process. At the load level of 7 tons and 12 tons (70 KN and 120 KN), the load in the grout did not transfer to the bottom of the anchor. Even at 15 tons (150 KN) load level, the average load from 6.16 ft to 10.00 ft (1.88 m to 3.00 m) was much smaller than that from 0 ft to 6.16 ft (0 m to 1.88 m). This indicated that the lower part of the anchor had the potential to bear a higher load.

Figures 4.12-4.14 are the shear stress distribution curves for anchors with different grouting materials. In general, the trend of shear stress distribution along the anchor shaft was similar to the load distribution curves. At lower load level of 5 tons and 7 tons (50 KN and 70 KN), the shear stress from 0 to 4 ft (0 m to 1.22 m) was the largest. While at middle load level of 12 ton (120 KN), the shear stress at 3.83 ft (1.17 m) was the largest. And at high load level of 15 ton (150 KN), the shear stress at 6.16 ft (1.88 m) was the largest.

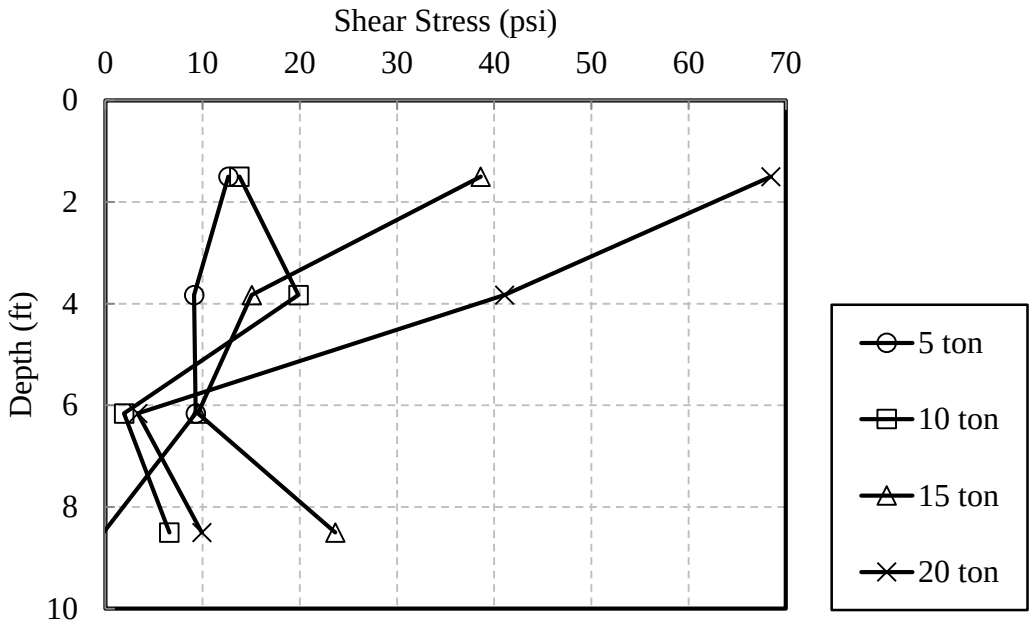

Figure 4.12 Shear Stress Distribution for Anchor Grouted with Microsil Anchor Grout (Anchor 3)

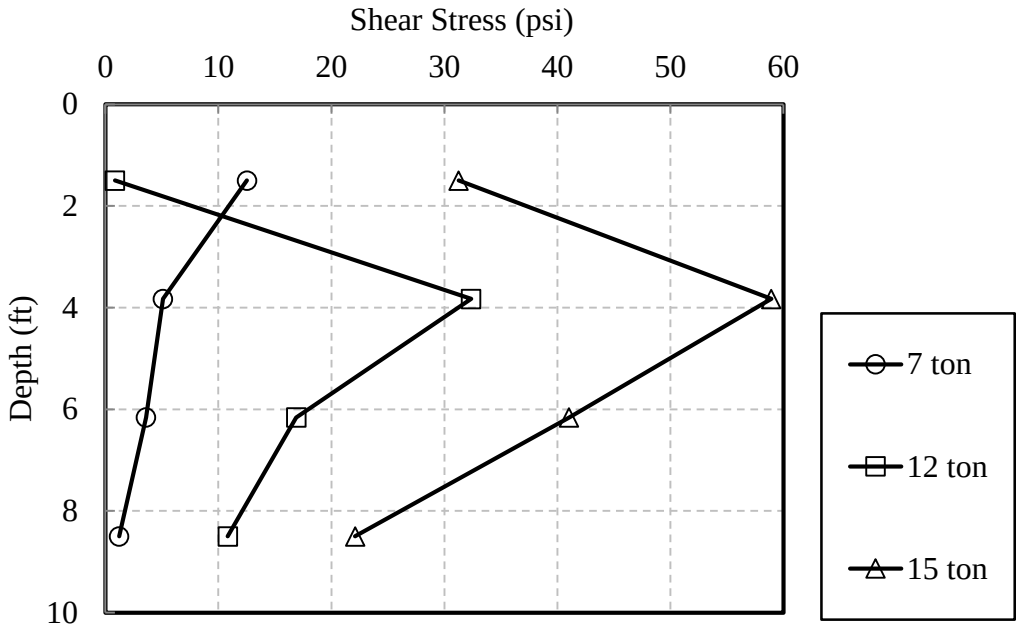

Figure 4.13 Shear Stress Distribution for Anchor Grouted with Bentonite Clay (Anchor 8)

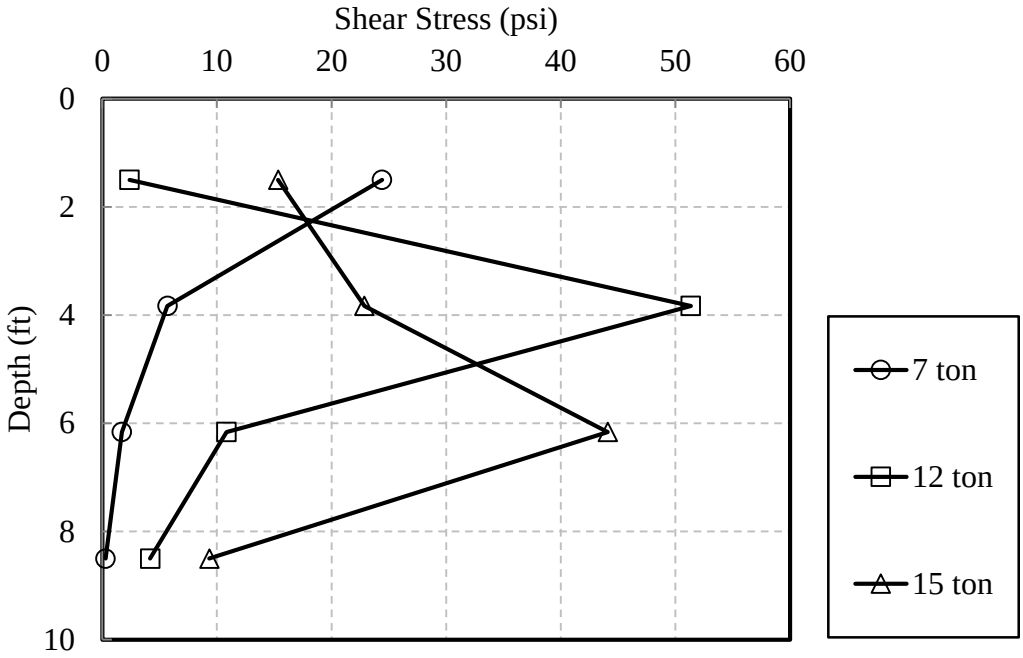

Figure 4.14 Shear Stress Distribution for Anchor Grouted with Antifreeze Grout Mortar (Anchor 11)

4.4 CREEP BEHAVIOR ANALYSES

4.4.1 Creep Curve Adjustment Procedures

As part of the testing program, it is necessary to measure the vertical movements of the anchor with respect to time. The creep test was supposed to be a constant load test. However, the hydraulic pump used in the field test could not maintain a constant load. This made it difficult to analyze the test results according to the conventional approach. Adjustment was therefore needed to facilitate data analyses. Two assumptions were made when adjusting the displacement versus load curves (Morgenstern et al., 1980; Nixon and McRoberts, 1976): (1) instantaneous strain is negligible for long-term creep test, and (2) Boltzmann superposition principle is valid. All of the raw displacement data was revised according to the procedures explained in the following sections.

The total ε strain of the anchor consists of two parts: instantaneous strain ε_0 and creep strain ε^c:

$$\varepsilon = \varepsilon_0 + \varepsilon^c \tag{4.11}$$

Andersland and Ladanyi (2004) pointed out that in practice, the instantaneous strain in the short-term is governed by Hooke's law, while the long-term instantaneous strain consists of elastic, plastic, and primary creep strains. The instantaneous strain is represented by one variable, called

the pseudo-instantaneous strain. This pseudo-instantaneous strain is defined as the value where the extension of the steady-state creep curve intersects with the strain axis. Similarly, Vialov (1959) also mentioned that the pseudo-instantaneous portion is less than 10% of the total strain when the testing time is greater than one day. Therefore, the instantaneous stress-strain relationship is expressed by Equation (4.12):

$$\varepsilon^e = \frac{\sigma}{E} \tag{4.12}$$

where ε^e is elastic strain; σ is applied stress; and E is Young's modulus.

The creep strain in Equation (4.11) is expressed as:

$$\varepsilon^c = \dot{\varepsilon}^c_{min} t \tag{4.13}$$

where ε^c is creep strain; $\dot{\varepsilon}^c_{min}$ is minimum strain rate; and t is time.

Therefore, the total strain ε is rewritten as follows:

$$\varepsilon = \frac{\sigma}{E} + \dot{\varepsilon}^c_{min} t \tag{4.14}$$

For engineering practice, the load history effect is often ignored during stress-strain analyses (Ladanyi, 1972). As a result, the Boltzmann superposition principle is valid and the following two equations hold true:

$$\varepsilon[c\sigma(t)] = c\varepsilon[\sigma(t)] \tag{4.15}$$

$$\varepsilon[\sigma_1(t)+\sigma_2(t-t`)] = \varepsilon[\sigma_1(t)] + \varepsilon[\sigma_2(t-t`)] \tag{4.16}$$

where ε is strain; σ is stress; c is a constant value; t is time; and t` is the time when stress starts to change.

Equations (4.15 and 4.16) indicate that for linear viscoelastic material, strain response due to complex loadings is equal to the sum of the strains induced by each loading independently. The stress input σ(t) is a function of time, and can be expressed:

$$\sigma(t) = \sum_{i=1}^{n} \Delta\sigma_i H(t - t_i) \tag{4.17}$$

where σ(t) is stress input function; *i* and *n* are the i^{th} time step and total time steps, respectively; $\Delta\sigma_i$ is stress change during i^{th} time steps; and $H(t-t_i)$ is time dependent function.

According to the Boltzmann superposition principle, the total strain for a number of stress inputs is equal to the sum of the strain output induced by each stress separately. Therefore, the total strain under various stress inputs is expressed as:

$$\varepsilon(t) = \sum_{i=1}^{n} \Delta\sigma_i H(t - t_i) J(t - t_i) \quad (4.18)$$

where $J(t\text{-}t_i)$ is creep compliance of the i^{th} time step.

In a summary, if the applied load is known, the corresponding elastic strain change can be found using Equation (4.12). Both the displacement and the applied load data were recorded every minute. For such a short time interval, the applied load was considered to be constant. The creep strain change during each time interval can be calculated by using Equation (4.13). Therefore, the compensated total strain can be determined by Equation (4.14). After individual segments of the strain curve were revised, the segments were assembled end-to-end to form the continuous time-strain curves. Finally, by multiplying the anchor length (10 ft or 120 in), the revised displacement curve was obtained. Based on the method discussed above, Figure 4.15 shows the typical displacement vs. time curve (creep curve) for one of the anchors tested, anchor 11. The jagged upper line in the figure shows that the difference between maximum and minimum loads could be larger than 3 ton (26.69 KN). The lower two lines are the displacement vs. time curves before and after adjustment.

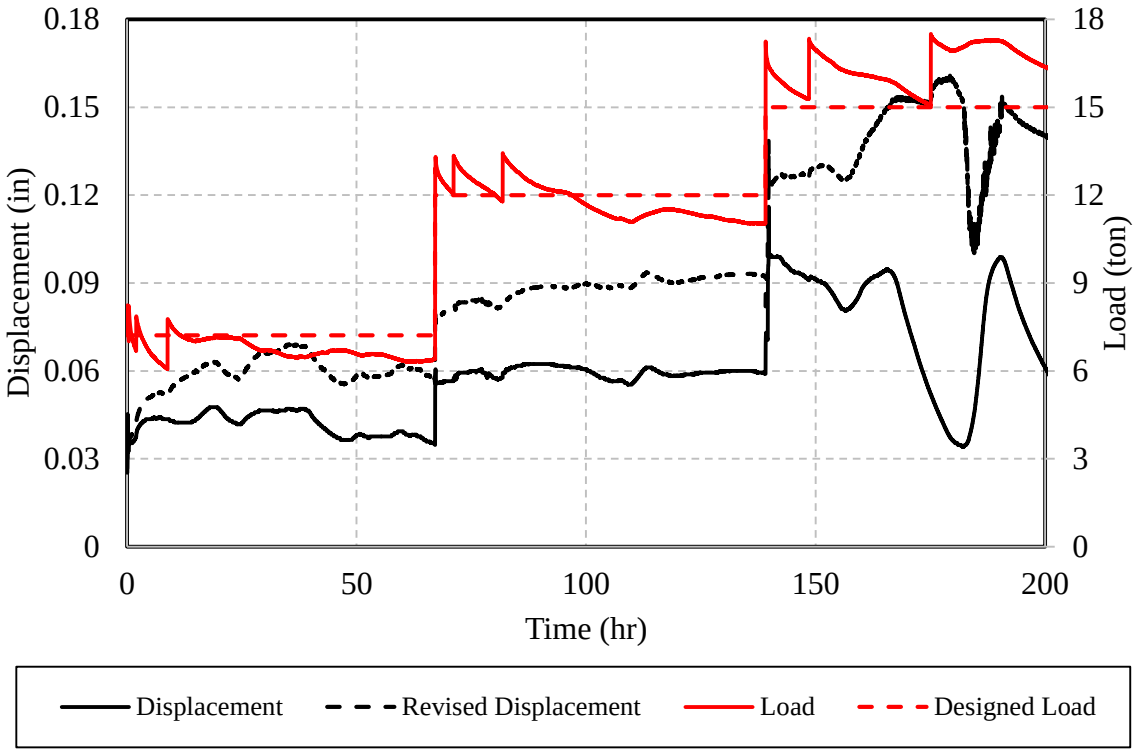

Figure 4.15 Typical Displacement vs. Time Curve

4.4.2 Creep Test Results and Discussions

The displacement vs. time curves for different anchors vary dramatically even if the grout materials are the same. Reasons for this could include:

1. Inconsistency of the soil profiles at different anchor locations. As discussed at the beginning of Chapter 4, the soil profiles contain various combinations of ice wedges, silt and gravel.
2. Gravel influence. For some anchor locations, gravel layers of varying thickness were noted.
3. Variable diameters of anchor boreholes. During the drilling process, the majority of the holes were expanded from a smaller (3 inch) predrilled hole. The diameter of holes could vary from hole to hole as well as vary somewhat within individual holes.
4. Adfreeze bond strength variations due to grout hydration heat. Adfreeze bonds between the grouted-filled anchor shafts and the native permafrost soils may have varied significantly due to the different amounts of hydration heat generated by the different grout types.

Figure 4.16 is the displacement vs. time curve for Anchor 4, which is solid tendon grouted with Microsil Anchor Grout. The average strain rates at 7 ton (62.3 KN), 12 ton (106.8 KN) and 15 ton (133.5 KN) were 7.066×10^{-5} hr^{-1}, 6.001×10^{-5} hr^{-1} and 5.660×10^{-5} hr^{-1}. The strain rates decreased with the increment of normal stress, which indicates one of the interesting properties of ice-rich soil. Pekarskaya (1965) mentioned before that ice was known to creep at low stresses. For ice-rich soil at higher stress conditions, ice itself could heal or restore the broken bonds during the strain process which would in turn slow down the speed of creep. This test result confirms his findings.

Another interesting finding is that the primary creep of undisturbed Fairbanks Silt is limited. At higher load levels, say 12 ton (106.8 KN) and 15 ton (133.5 KN), the primary creep was not obvious. Thompson and Sayles (1972) also pointed out that this phenomenon was maintained for strains exceeding 20%. And a stress exponent of 4 that was determined for higher stress levels that agreed with other researchers' results (Butkovich and Landaucer, 1959 and 1960, Morgenstern et al., 1980).

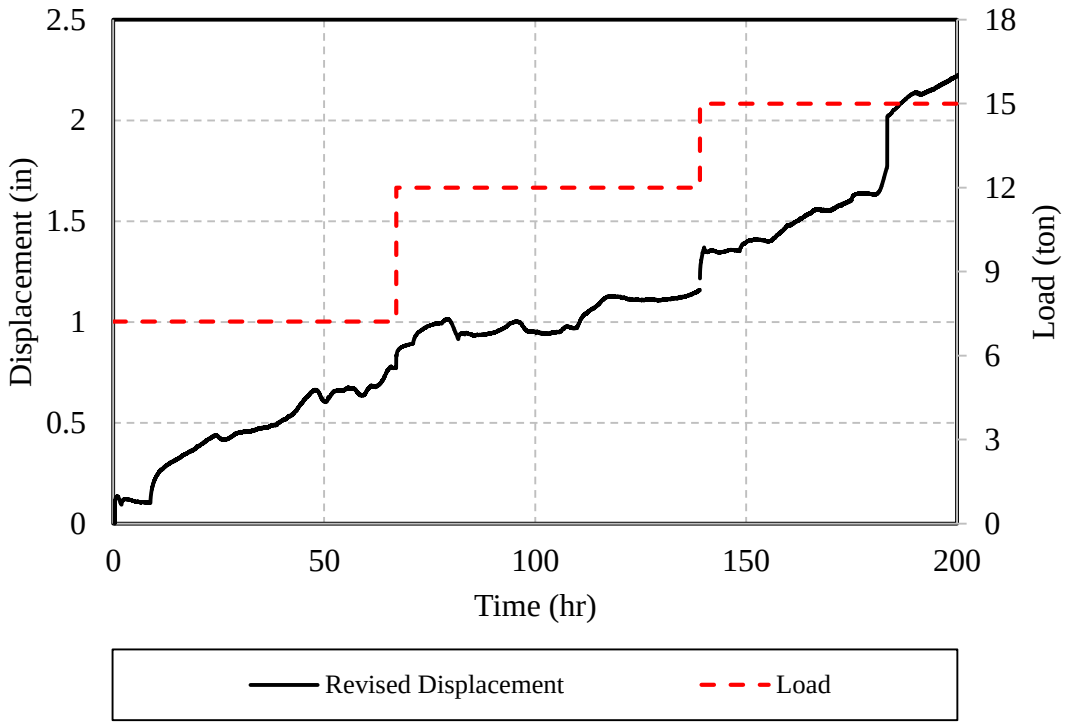

Figure 4.16 Displacement vs. Time for Anchor with Microsil Anchor Grout (Anchor 4)

Figure 4.17 presents the displacement vs. time curve for anchor 10, which is a hollow tendon grouted with Bentonite Clay. The average strain rates at 7 ton (62.3 KN), 12 ton (106.8 KN) and 15 ton (133.5 KN) were 1.552×10^{-5} hr^{-1}, 1.291×10^{-5} hr^{-1} and 5.956×10^{-6} hr^{-1} respectively. In general, the strain rates for anchor 10 were much smaller than those of anchor 4. The anchor experienced a large strain as load increment was added, but rapidly went into a low rate of secondary creep. No tertiary creep stage was observed during the test.

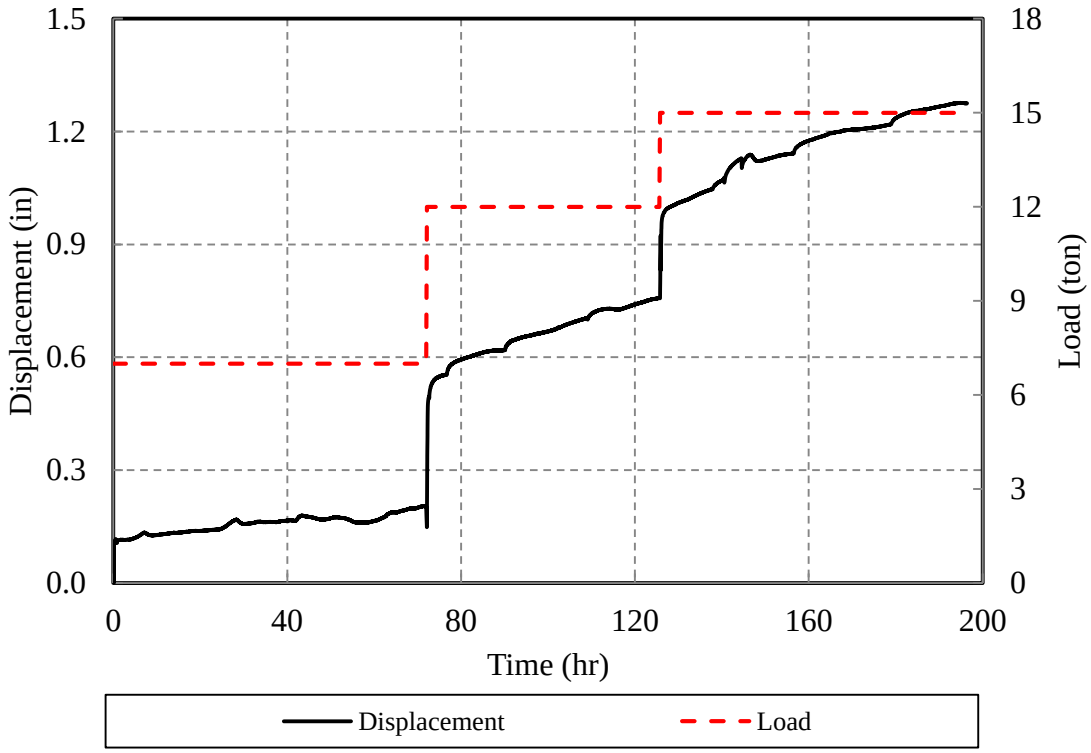

Figure 4.17 Displacement vs. Time Curve for Anchor with Bentonite Clay (Anchor 10)

Figure 4.18 shows the displacement vs. time curve for anchor 12, which is a hollow tendon grouted with Antifreeze Grout Mortar. The average strain rates at 7 ton (62.3 KN), 12 ton (106.8 KN) and 15 ton (133.5 KN) were 5.261×10^{-6} hr^{-1}, 1.991×10^{-6} hr^{-1} and 7.326×10^{-7} $hr^{-1,}$ respectively. The strain rates for anchor 12 were much smaller than anchors 4 and 10.

In a summary, the total displacements varied from 0.157 in (4 mm) to 2.362 in (60 mm). The strain rates varied from 10^{-5} min^{-1} to 10^{-6} min^{-1}. The average strain rate at different load level can be considered fairly linear.

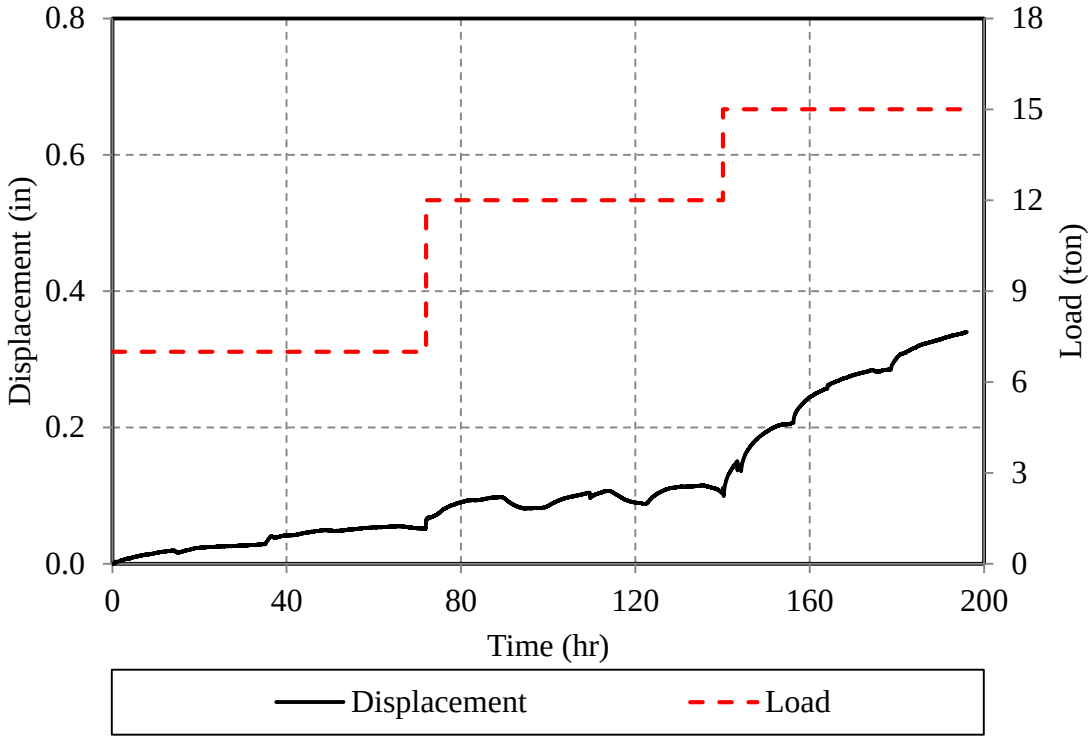

Figure 4.18 Displacement vs. Time Curve for Anchor with Antifreeze Grout Mortar (Anchor 12)

4.5 PULLOUT TEST RESULTS AND DISCUSSIONS

Among all the 13 anchors, only the anchors grouted with Bentonite Clay were pulled out and the ultimate pullout capacity was 35 ton (350 KN). At 35 ton (350 KN) load level, two phenomena indicated the anchor failure: displacement records kept continuously increasing and the hydraulic pump lost pressure dramatically. Figure 4.19(a) shows the mode for anchor 4 after failure. The failure occurred at the interface between grout and anchor tendon.

Figures 4.19 (a), (b) and (c) show the final appearances of anchors 4, 6 and 12 after pullout test. Anchors grouted with Microsil Anchor Grout and Antifreeze Grout Mortar did not fail at 55 ton (550 KN) load level. Several iron plates were broken after the pullout test due to extremely high pressure (about 9000 psi). For anchor 12, it seemed that it was uplifted by about 1 in. In fact, before the creep test, the ground was not flat and some of the frozen soil had been removed. So it gave an illusion that the anchor had been pulled out.

(a) (b) (c)

Figure 4.19 Anchors after Pullout Test

Figure 4.20 shows pullout test results for different grouting materials. The applied load interval was 5 tons and lasted for 5 minutes. As shown in the figure, the displacement curves for the anchors have been revised by subtracting the displacement induced by the settlement of the loading system. During the pullout test, only anchors grouted with Bentonite Clay were pulled out at 35 ton (350 KN). The maximum displacements for three types of grouting materials were 0.89 in (22.61 mm) for Microsil Anchor Grout, 1.52 in (38.61 mm) for Bentonite Clay and 1.27 in (33.26 mm) for Antifreeze Grout Mortar. Even though the total displacement for Antifreeze Grout Mortar was larger than that of Microsil Anchor Grout by 0.39 in (9.91 mm), the average displacement rates were at the same magnitude. Anchor grouted with Bentonite Clay failed at the load level of 35 ton (350 KN) without any indication and the average displacement rate was 2.16×10^{-2} in/min.

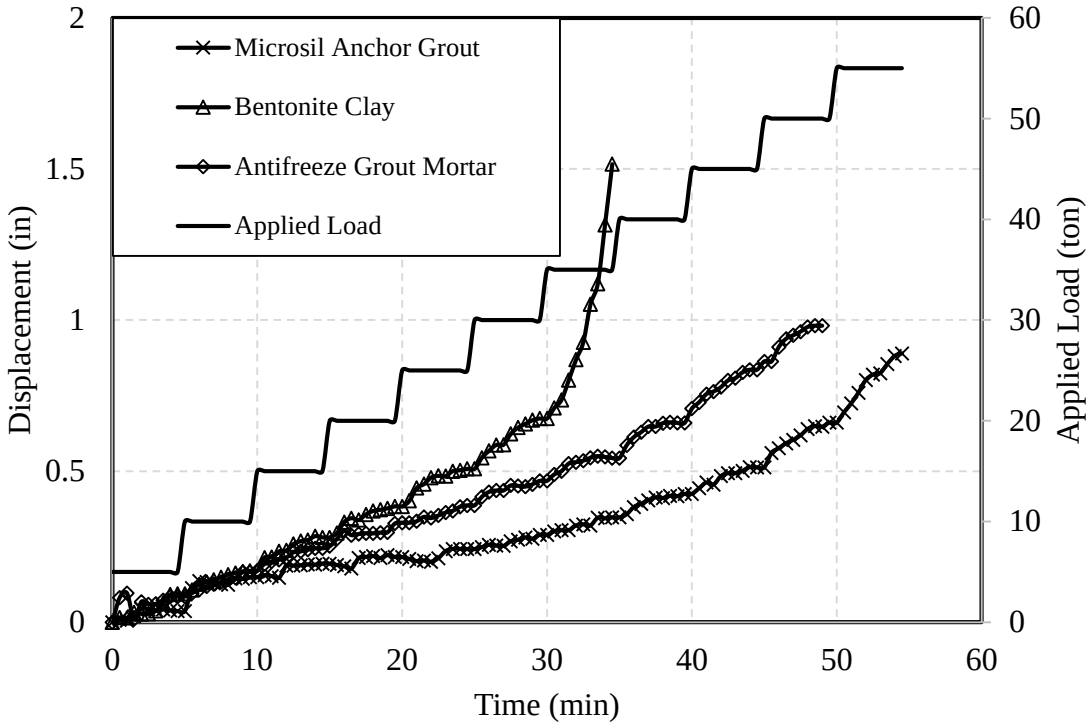

Figure 4.20 Pullout Test Results

CHAPTER 5 CONCLUSIONS AND RECOMMENDATIONS

This chapter presents a summary of the research based on field tests. Recommendations that address future needs and practical aspects of using shallow anchors in ice-rich permafrost are offered.

5.1 CONCLUSIONS

The major findings of the study are as follows:

1. The analysis of grouting temperature indicates that the average period of temperature above 32 ºF (0 ºC) is 4-5 hours. Both the short-term and long-term temperature monitoring results indicate that anchors grouted with Antifreeze Grout Mortar exhibited the least permafrost degradation, and took the least time to freeze back to initial temperature among all three grouting materials.
2. Both short-term and long-term load test results for duckbill anchors indicated very limited creep displacement. Most of the displacements measured during duckbill anchor testing were considered to be the result of cable stretching. It is recommended that duckbill anchors be installed by predrilling a borehole, backfilling with gravel, and grouting with water. This installation technology is much easier and still leads to satisfactory results.
3. The load redistribution along the anchor shaft largely depends on the type of grouting materials. Microsil Anchor Grout cracked when the applied load reached 15 ton (133.5 KN). Bentonite Clay cracked at the start of 7 ton (62.3 KN) load level. Neither the Microsil Anchor Grout nor the Bentonite Clay could bear large tensile loads, while Antifreeze Grout Mortar showed no crack up to 15 ton (133.5 KN).
4. The total displacements of all grouted anchors after 9 days of continuous load testing (3 days at 7 ton + 3 days at 12 ton + 3 days at 15 ton) were measured. Large variation in the results were found when displacements ranged from 0.157 in (4 mm) to nearly 2.36 in (60 mm). Many factors could have contributed to this large variation such as the inconsistency of borehole diameter, inconsistency of soil profile, and different properties of backfill materials.
5. Only anchors grouted with Bentonite Clay failed at 35 ton (350 KN) load level. The failure occurred at the interface with anchor tendon and grout. All other anchors were tested to 55 ton (550 KN) and no failure was observed.

In a summary, comparison of the field performance of three different types of grouting materials indicates that the Antifreeze Grout Mortar shows the least disturbance of the surrounding permafrost, gives the highest tensile strength, and exhibits smaller creep

displacement. Therefore, the shallow anchor grouted with Antifreeze Grout Mortar shows the best field performance and is applicable to ice-rich permafrost.

5.2 RECOMMENDATIONS

1. Use care in applying the results of this study. The study specifically focused on the performance of specific anchor and grout types installed in ice-rich silt. Findings of this research do not pertain to all anchor types in all soils. Further investigation is required to determine the performance of different types of soils.
2. The duckbill anchors were first placed in pre-drilled holes. Then, after trying several different methods of "setting" the anchors by applying load, the installation was finally accomplished by simply filling the pre-drilled hole (after the duckbill had been placed at the bottom of the hole) with gravel and water, and allowing time for freeze back. This installation technology is much easier and still leads to satisfactory results.
3. Ignore primary creep for the anchor and soil types addressed in this research. Primary strain was found to constitute less than 10 percent of the total strain. Moreover, using the strain rates of high load level to determine the total displacement will result in a non-conservative design. Do not use anchor displacement estimates based only on tests at high load levels for design purposes. Design assumptions based on load tests only at high loadings may be non-conservative.
4. Loads should not be applied to anchors in ice-rich permafrost within 5 days of grouting. This study indicated that, during the grouting process, the soil in the immediate vicinity of the anchor experiences 4-5 hours of temperature above 0ºC. Project data indicated that 3-5 days were required (conservatively) for the soil temperature to get back to its initial condition.
5. The pullout capacity of the shallow anchors is based on short term pullout test (at time interval of 5 min for each load level). The long-term capacity might be significantly smaller than short-term strength. Special attention should be paid to design the capacity of permanent grouted anchors based on short-term pullout test.
6. This thesis does not consider the effect of soil types on the creep and load distribution behavior. Since the friction shear stresses provided by frozen soils, ice and silt can vary significantly, more research is needed in this direction.

REFERENCES

Adams, D. A., and Littlejohn, G. S. (1997). "Anchorage Load Transfer Studies Using an Instrumented Full Scale Reusable Laboratory Apparatus." *Proceedings, International Conference Ground Anchorages and Anchored Structures*, London, UK, March 20-21, 411-421.

Adams, J. I., and Hayes, D. C. (1967). "The Uplift Capacity of Shallow Foundation." *Ontario Hydro Research Quarterly*, 19(1): 1-13.

Adams, J. L., and Klym, T. W. (1972). "A Study of Anchorages for Transmission Tower Foundations*." Canadian Geotechnical Journal*, 9(1): 89-104.

Andersland, O. B., and Ladanyi, B. (2004). "Frozen Ground Engineering, 2nd Edition." *John Wiley & Sons,* Hoboken, New Jersey, 106-135.

Arenson, L. U., and Springman, S. M. (2005). "Mathematical Description for the Behavior of Ice-Rich Frozen Soils at Temperatures Close to Zero Centigrade." *Canadian Geotechnical Journal*, 42(2): 431-442.

Barley, A. D. (1997). "The Single Bore Multiple Anchor System." *Proceedings, International Conference Ground Anchorages and Anchored Structures*, London, UK, March 20-21, 65-75.

Barnes, J. A., CHI, A. R., Cutler, L. S., Healey, D. J., Lesson, D. B., McGunigal, T. E., Mullen, J. A., Smith, W. L., Sydnor, R., Vessot, R. F., and Winkler, G. M. R. (1971). Charaterization of Frequency Stability." *IEEE Transactions on Instrumentation and Measurement*, IM-20: 105-120.

Bhatnagar, R. S. (1969). "Pullout Resistance of Anchors in Silty Clay." *M. S. Thesis*, Duke University, Durham, N. C., USA.

Biggar, K. W. (1991). "Adfreeze and Grouted Piles in Saline Permafrost." *Ph. D. Thesis,* University of Alberta, Canada, 449.

Biggar, K. W., and Kong, V. (2001). "An Analysis of Long-Term Pile Load Tests in Permafrost from the Short Range Radar Site Foundations." *Canadian Geotechnical Journal*, 38(3): 441-460.

Biggar, K. W., and Sego, D. C. (1990). "The Curing and Strength Characteristics of Cold Setting Cement Fondu Grout." *Proceedings, 5th Canadian Permafrost Conference*, Winnipeg, Manitoba, Canada, 304-312.

Biggar, K. W., and Sego, D. C. (1993a). "Field Pile Load Tests in Saline Permafrost. I: Test procedures and results." *Canadian Geotechnical Journal*, 30(1): 34-45.

Biggar, K. W., and Sego, D. C. (1993b). "Field Pile Load Tests in Saline Permafrost. II: Analysis of Results." *Canadian Geotechnical Journal*, 30(1): 46-59.

Biggar, K. W., Sego, D. C., and Noel, M. M. (1991). "Laboratory and Field Performance of High Alumina Cement Based Grout for Piling in Permafrost." *44th Canadian Geotechnical Conference*, Calgary, Alberta, Canada, 42.

Bray, M. T. (2008). "The Influence of Soil Cryostructure on the Creep and Long-Term Strength Properties of Frozen Soils." *Ph.D. Thesis*, University of Alaska Fairbanks, AK, US, 22-25.

Briaud, J. L., Powers, W. F., and Weatherby, D. E. (1998). "Should Grouted Anchors Have Short Tendon Bond Length?" *Journal of Geotechnical and Geoenvironmental Engineering, ASCE,* 124(2): 110-119.

Budd, W. F. (1969). "The Dynamics of Ice Masses." *ANARE Scientific Reports*, Series A(IV), Glaciology, 108.

Butkovich, T. R. (1954). "Hardness of Single Ice Crystals." *Snow, Ice and Permafrost Research Establishment (SIPRE),* Corps of Engineers, U. S. Army, Research Report No.9: 12.

Butkovich, T. R., and Landauer, J. K. (1959). "The Flow Law for Ice." *Cold Regions Research and Engineering Laboratory (CRREL),* Hanover, New Hampshire, Research Report 56.

Butkovich, T. R., and Landauer, J. K. (1960). "Creep of Ice at Low Stresses." *Snow, Ice and Permafrost Research Establishment (SIPRE),* Corps of Engineers, U. S. Army, Research Report 72.

Butterfield, R., and Banerjee, P. K. (1971). "The Problem of Pile Group and Pile Cap Interaction." *Geotechnique,* 21(2): 135-142.

Casanovas, J. S. (1989). "Bond Strength and Bearing Capacity of Injected Anchors: A New Approach." *Proceeding of the 12th Conference, Soil Mechanics and Foundation Engineering,* Rio de Janeiro, Brazil, 1005-1008.

Cook, R. A., Kunz, J., Fuchs, W., and Konz, R. (1998). "Behavior and Design of Single Adhesive Anchors Under Tensile Load in Uncracked Concrete." *ACI Structural Journal,* ACI, 95(1): 9-26.

D'Appolonia, E., and Romualdi, J. P. (1963). "Load Transfer in End-Bearing Steel H-Piles." *Journal of the Soil Mechanics and Foundations Division,* Proceedings of the ASCE, No. SM2: 1-25.

Das, B. M. (1975). "Pullout Resistance of Vertical Anchors." *Journal of Geotechnical Engineering, ASCE,* 101(1): 87-91.

Desai, C. S. (1974). Numerical Design-Analysis for Piles in Sands." *Journal of the Geotechnical Engineering Division,* Proceedings of the ASCE, Vol. 100, No. GT6: 613-635.

Ellison, R. D., D'Appolonia, E., and Thiers, G. R. (1971). "Load-Deformation Mechanism for Bored Piles." *Journal of the Soil Mechanics and Foundations Division*, Proceedings of the ASCE, Vol. 97: SM4.

Glen, J. W. (1952). "Experiments on the Deformation of Ice." *Journal of Glaciology*, 2(12): 111-114.

Glen, J. W. (1955). "The creep of polycrystalline ice." *Proceeding of the Royal Society*, London, UK, A (228), 519-538.

Hanna, A., Ayadat, T., and Sabry, M. (2007). "Pullout Resistance of Single Vertical Shallow Helical and Plate Anchors in Sand." *Geotechnical and Geological Engineering*, 25(4): 559-573.

Hsu, S. (2012). "Behavior of Pressure-Grouted Anchors in Gravel." *Canadian Geotechnical Journal*, 49(6): 719-728.

Hutchinson, D. J. (1989). "Model Pile Load Test in Frozen Saline Silty Sand." *M. S. Thesis*, University of Alberta, Edmonton, Canada.

Johnston, G. H., and Ladanyi, B. (1972). "Field Tests of Grouted Rod Anchors in Permafrost." *Canadian Geotechnical Journal*, 9(2): 176-194.

Jorgenson, T., Yoshikawa, K., Kanevskiy, M., Shur, Y., Romanovsky, V., Marchenko, S., Grosse, G., Brown, J., and Jones, B. (2008). "Permafrost Characteristics of Alaska." *Institute of Northern Engineering, University of Alaska Fairbanks*, AK, US.

Kanevskiy, M., Fortier, D., Shur, Y., Bray, M. T., and Jorgenson, T. (2008). "Detailed Cryostratigraphic Studies of Syngenetic Permafrost in the Winze of the CRREL Permafrost Tunnel, Fox, Alaska." *Proceedings, 9th International Conference on Permafrost*, Fairbanks, AK, US, June 29-July 3, 889-894.

Ladanyi, B., and Johnston, G. H. (1974). "Behavior of Circular Footings and Plate Anchors Embedded in Permafrost." *Canadian Geotechnical Journal*, 11(4): 531-553.

Leung, Y. F., Klar, A. and Soga, K. (2010). "Theoretical Study on Pile Length Optimization of Pile Groups and Pile Rafts." *Journal of Geotechnical and Geoenvironmental Engineering*, 136(2): 319-330.

Ladanyi, B. (1972). "An Engineering Theory of Creep of Frozen Soils." Canadian Geotechnical Journal, 9(1): 63-80.

Lin, C., Liu, J., and Zhang, X. (2015). "Development of Innovative Antifreeze Grout Mortar for Anchor Application in Cold Regions." *Transportation Research Board 94th Annual Meeting*, Washington, D. C., US, January 11-15. (Accepted for Publication)

Mattes, N. S. (1969). “The Influence of Radial Displacement Compatibility on Pile Settlements.” *Geotechnique*, Vol. 20:157-159.

McRoberts, E. C., Law, T. C., and Murray, T. K. (1978). “Creep Tests on Undisturbed Ice-Rich Silt.” *Proceedings, 3rd International Conference on Permafrost*, Edmonton, Alberta, Canada, July 10-13, 539-545.

Mellor, M., and Testa, R. (1969). “Effect of Temperature on the Creep of Ice.” *Journal of Galciology*, 8(52): 131-145.

Mindlin, R. D. (1936). “Force at a Point in the Interior of a Semi-Infinite Solid.” *Physics*, 7(5): 195-202.

Morgenstern, N. R., Roggensack, W. D., and Weaver, J. S. (1980). “The behavior of Friction Piles in Ice and Ice-Rich Soils.” *Canadian Geotechnical Journal*, 17(3): 405-415.

Mylonakis, G., and Gazetas, G. (1998). “Settlement and Additional Internal Forces of Grouped Piles in Layered Soil.” *Geotechnique,* 48(1): 55-72.

Nixon, J. F. (1988). “Pile Load Tests in Saline Permafrost at Clyde River, Northwest Territories.” *Canadian Geotechnical Journal*, 25(1): 24-32.

Nixon, J. F., and Neukirchner, R. J. (1984). “Design of Vertical and Laterally Loaded Piles in Saline Permafrost.” *Proceedings, 3rd International Specialty Conference on Cold Regions Engineering*, Edmonton, Alberta, Canadian Society of Civil Engineering, April 1-6, 131-144.

Nixon, J. F., and McRoberts, E. C. (1976). “A Design Approach for Pile Foundations in Permafrost.” *Canadian Geotechnical Journal*, 13(40): 40-57.

O’Neill, M. W., and Reese, L. C. (1970). “Behavior of Axially Loaded Drilled Shafts in Beaumont Clay.” *Center for Highway Research,* University of Texas at Austin, Research Report 89-8, Parts 1-5.

Parmeswaran, V. R. (1986). “Bearing Capacity Calculations for Piles in Permafrost.” *Proceedings, 4th International Conference Cold Regions Engineering*, TCCRE, ASCE, Anchorage, AK, February 24-26, 751-759.

Paterson, W. S. B., and Savage, J. C. (1963). “Geometry and Movement of Athabasca Glacier.” *Journal of Geophysical Research*, 68(15): 4513-4520.

Poulos, H. G., and Davis, E. H. (1968). “The Settlement Behavior of Axially Loaded Incompressible Piles and Piers.” *Geotechnique,* 18(3): 351-371.

Randolph, M. F., and Wroth, C. P. (1979). "Driven Piles in Clay-the Effects of Installation and Subsequent Consolidation." *Geotechnique,* 29(4): 361-393.

Raymond, C. F. (1971). "Flow in a Transverse Section of Athabasca Glacier, Alberta, Canada." *Journal of Glaciology*, 10(58): 55-84.

Roggensack, W. D. (1977). "Geotechnical Properties of Fine-Grained Permafrost Soils." *Ph. D. Thesis,* University of Alberta, Canada, 449.

Rollins, K. M., Clayton, R. G., Mikesell, R. C., and Blaise, B. C. (2005). "Drilled Shaft Side Friction in Gravelly Soils." *Journal of Geotechnical and Geoenvironmental Engineering, ASCE,* 131(8): 987-1003.

Sayles, F. H. (1968). "Creep of Frozen Sands." *Cold Regions Research and Engineering Laboratory (CRREL),* Hanover, New Hampshire, Research Report No. 190: 54.

Sego, D. C., and Smith, L. B. (1989). "Effect of backfill Properties and Surface Treatment on the Capacity of Adfreeze Pipe Piles." *Canadian Geotechnical Journal*, 26(4): 718-725.

Shreve, R. L., and Sharp, R. P. (1970). "Internal Deformation and Thermal Anomalies in Lower Blue Glacier, Mount Olympus, Washington, U. S. A.." *Journal of Glaciology*, 9(55): 65-86.

Subramanian, N., and Cook, R. A. (2002). "Installation, Behavior and Design of Bonded Anchors." *The Indian Concrete Journal*, 76(1): 1-10.

Subramanian, N., and Cook, R. A. (2004). "Behavior of Grouted Anchors." *The Indian Concrete Journal,* 78(4):14-21.

Thomas, R. H. (1973). "The Creep of Ice Shelves: Theory." *Journal of Glaciology,* 12(64): 45-53.

Thompson, E. G., and Sayles, F. H. (1972). "In Situ Creep Analysis of Room in Frozen Soil." *Journal of the Soil Mechanics and Foundations Division*, 98(9): 899-915.

Vesic, A. S. (1969). "Experiments with Instrumented Pile Groups in Sand." *Performance of Deep Foundations, ASTM*, Spec. Tech. Publ. No. 444, 177-222.

Vialov, S. S. (1959). "Rheological Properties and Bearing Capacity of Frozen Soils." *Cold Regions Research and Engineering Laboratory (CRREL),* Hanover, New Hampshire, Technical Translation No. 74: 219.

Vialov, S. S., Gmoshinskii, V. G., Gorodetskii, S. E., Grigorieva, V. G., Zaretskii, I. K., Perkarskaya, N. K., and Shusherina, E. P. (1962). "The Strength and Creep of Frozen Soils and

Calculations for Ice-Retaining Structures." *Cold Regions Research and Engineering Laboratory (CRREL),* Hanover, New Hampshire, Technical Translation No. 76: 301.

Weaver, J. S. (1979). "Pile Foundations in Permafrost." *Ph.D. Thesis,* University of Alberta, Edmonton, Canada.

Zhu, Y., and Carbee, D. L. (1987). "Tensile Strength of Frozen Soil." *Cold Regions Research and Engineering Laboratory (CRREL),* Hanover, New Hampshire, Research Report, 87: 15.